

21st Century Projections of Snowfall and Winter Severity Across Central-Eastern North America

Michael Notaro and David Lorenz

Nelson Center for Climatic Research
University of Wisconsin-Madison

1225 West Dayton Street, Madison, Wisconsin 53706

Correspondence: mnotaro@wisc.edu, phone 608-261-1503, fax 608-263-4190

Christopher Hoving

Michigan Department of Natural Resources – Wildlife Division, Lansing, Michigan

Michael Schummer

Long Point Waterfowl, Port Rowan, Ontario

Current address: Department of Biological Sciences, State University of New York at Oswego,
Oswego, New York

Keywords: Snow projection, climate change, statistical downscaling, Landscape Conservation Cooperatives, winter severity index

Abstract

Statistically downscaled climate projections from nine global climate models (GCMs) are used to force a snow accumulation and ablation model (SNOW-17) across the central-eastern North American Landscape Conservation Cooperatives (LCCs) to develop high-resolution projections of snowfall, snow depth, and winter severity index (WSI) by the mid- and late 21st century. Decreasing temperature and increasing snow depth influence survival and distribution of wildlife that are important to North America's ecology, environment, culture, and economy. Here, we use projections of a cumulative WSI (CWSI) known to influence autumn-winter waterfowl migration to demonstrate the utility of SNOW-17 results. The application of statistically downscaled climate data and a snow model leads to a better representation of lake processes in the Great Lakes Basin, topographic effects in the Appalachian Mountains, and spatial patterns of climatological snowfall, compared to the original GCMs. Annual mean snowfall is simulated to decline across the region, particularly in December-January, implying a delayed snow season. Due to a warming-induced acceleration of snowmelt, the percentage loss in snow depth exceeds that of snowfall. Across the Plains and Prairie Potholes LCC and Upper Midwest and Great Lakes LCC, daily snowfall events are projected to become less common, but more intense. The greatest reductions in the number of days per year with a present snowpack are expected close to the historical position of the -5°C isotherm in DJFM, around 44°N. The CWSI is projected to decline substantially during December-January, leading to increased likelihood of delays in timing and intensity of autumn-winter waterfowl migrations, enhanced white-tailed deer survival rates, and altered predator-prey relationships.

70

71

72 1. Introduction

73 Snow is an important element of the hydrologic cycle, replenishing soil moisture and
74 contributing runoff to river basins through spring melt (Lettenmaier and Gan 1990; Groisman et
75 al. 2001). The presence of snow cover leads to enhanced longwave emissivity and an insulating
76 effect on soil temperatures (Zhang et al. 2008). Continued increasing temperatures may lead to a
77 diminished snowpack, which would shift snowmelt from spring to winter (Manabe et al. 1981;
78 Mahanama et al. 2011), reduce soil moisture in spring-summer during the low-flow season
79 (Mastin et al. 2011), favor drought development (Mishra et al. 2010; Mahanama et al. 2011), and
80 increase fire risk (Westerling et al. 2006). Furthermore, snow influences many facets of society.
81 Spring snowpack is an essential water-supply reservoir for irrigation, hydroelectric power
82 generation, and municipal demands (Norton and Bolsenga 1993; Kunkel et al. 2000; Christensen
83 et al. 2004; Barnett et al. 2005; Vicuna et al. 2008). Snowfall supports multi-million dollar
84 winter recreational industries and tourism (Scott et al. 2008). Heavy snowstorms can be a
85 natural hazard to life and property, leading to automobile accidents (Eisenberg and Warner 2005),
86 heart attacks (Rogot and Padgett 1976), disrupted air and surface traffic (Robinson 1989;
87 Rasmussen et al. 1993), and large economic costs (Rooney 1967).

88 Survival and distribution of many animals are strongly impacted by the presence and
89 depth of snow (Notaro et al. 2011). The primary stressors to white-tailed deer are air chill and
90 snow hazard, with the presence of snow contributing to heat loss in deer, reduced mobility, and
91 elevated mortality rates (Severinghaus 1947; Edwards 1956; Verme 1968). The snowshoe hare
92 and ermine rely on snow cover for winter camouflage from predators. Snow cover regulates
93 predator-prey relationships, with a loss of snowpack reducing the competitive advantage of
94 American marten and Canada lynx (Krohn et al. 2004; Hoving et al. 2005; Carroll 2007).

95 The Winter Severity Index (WSI), developed as a cumulative measure of winter air chill
96 and snow hazard, is a key operation tool used by the Department of Natural Resources for
97 wildlife conservation. Verme (1968) designed a WSI that addresses the winter stresses of
98 northern deer in Michigan, based on calorimeters and snow depth. Kohn (1975) introduced a
99 Wisconsin-specific WSI, based on summing the number of days with a minimum temperature of
100 -17.8°C (0°F) or less and the number of days with at least 45.7 cm (18 inches) of snow on the
101 ground; the winter air-chill metric and the snow hazard metric were added together from 1
102 December to 30 April to compute the seasonal WSI.

103 Schummer et al. (2010) developed a cumulative winter severity index (CWSI) to explain
104 changes in the relative abundance of dabbling ducks during autumn-winter at mid-latitude
105 migration areas of eastern North America. CWSI is defined as:

$$106 \quad \text{CWSI} = \text{TEMP} + \text{TEMPDAYS} + \text{SNOW} + \text{SNOWDAYS} \quad (1)$$

107 where TEMP is the mean daily temperature ($^{\circ}\text{C} * -1$), TEMPDAYS is the number of consecutive
108 days with a mean temperature less than 0°C , SNOW is the snow depth (cm/2.54), and
109 SNOWDAYS is the number of consecutive days with a snow depth of at least 2.54 cm. CWSI is
110 cumulatively summed each day from 1 September to 31 March. For temperate regions, CWSI
111 remains below zero throughout the warm season, but as the air temperature consistently drops
112 below freezing and a snowpack develops in late autumn-early winter, the index accrues and
113 achieves positive values. CWSI reflects the current and cumulative effects of temperature on
114 ducks' energy expenditure and snow and ice cover on food availability to meet the ducks' energy
115 needs. Based on threshold CWSI values of 7.2 for mallards and -4.6 for other dabbling ducks,
116 researchers can identify the likely date when duck abundance will begin to decrease at northern
117 latitudes with southward migration (Schummer et al. 2010).

118 North American snow cover has declined since the mid-20th century, especially in spring
119 (Brown 2000; Lemke et al. 2007). Snow cover duration across the Northern Hemisphere
120 decreased during 1966-2007 across a zone where the seasonal mean air temperatures were within
121 -5°C to 5°C (Brown and Mote 2009). In contrast, a diminishing lake ice cover and more
122 favorable circulation patterns have enhanced lake-effect snowfall across the Great Lakes Basin
123 (Norton and Bolsenga 1993; Leathers and Ellis 1996; Burnett et al. 2003). If no change is
124 expected in precipitation, then a future temperature increase should favor more rain and less
125 snow. However, given projections of greater cold season precipitation, particularly at the mid-
126 high latitudes, an increase in snowfall might be expected where temperature continues to remain
127 below freezing (Kapnick and Delworth 2013). The response in snow cover to enhanced
128 greenhouse warming is therefore complicated by projected increases in mid-high latitude
129 precipitation, such that the response could vary by latitude and elevation (Groisman et al. 1993;
130 Räisänen 2007; Brown and Mote 2009). Climate models generally display a transition zone,
131 around the present-day -10°C isotherm, with expected increases in snowfall to the north (high
132 latitudes) and decreases to the south (mid-latitudes) (Krasting et al. 2013). Projections of snow
133 depth are more complicated than of snowfall, as the former is determined by both snowfall and
134 snowmelt-driven runoff and sublimation (Kapnick and Delworth 2013).

135 Several modeling studies have generated coarse projections of 21st century snowfall.
136 Long-term planning for water management strategies and reservoir design is driven by the
137 potential for greater winter flows and reduced spring snowpack and spring-summer runoff
138 (Adeloye et al. 1999; Draper and Kundell 2007; Mastin et al. 2011). Simulations by the National
139 Center for Atmospheric Research (NCAR) Community Climate System Model suggest that snow
140 cover will decline across all of North America, except northernmost Canada, during the 21st

141 century, particularly during springtime, despite projected increases in cold season precipitation
142 (Peacock 2012). Using another global climate model (GCM), Kapnick and Delworth (2013)
143 simulated positive trends in 21st century snowfall across the mid-high latitudes and negative
144 trends across the low-mid latitudes, including reductions across all of North America, except
145 Hudson Bay and northern Quebec. According to an ensemble of coupled atmosphere-ocean
146 GCMs from the Coupled Model Intercomparison Project Phase Five (CMIP5), annual snowfall is
147 anticipated to decline during the 21st century across much of the Northern Hemisphere, except
148 with high-latitude increases (Brutel-Vuilmet et al. 2013; Krasting et al. 2013). The CMIP3 and
149 CMIP5 GCMs share similar deficiencies in terms of their ability to simulate mean patterns and
150 trends in Northern Hemispheric snow cover, including an underestimation of the recent negative
151 trend in spring snow cover extent (Roesch 2006; Brutel-Vuilmet et al. 2013).

152 The purpose of this study is to generate high-resolution projections of daily snowfall,
153 snow depth, and winter severity index for the mid- and late 21st century across the central-eastern
154 North American Landscape Conservation Cooperatives (LCCs) using an operational snow model
155 forced by statistically downscaled CMIP3 climate projections. The LCCs are an applied
156 conservation science partnership among states, federal agencies, universities, non-governmental
157 organizations, and tribes that provides the expertise needed to support conservation planning at
158 the landscape scale. These snow and winter severity projections will benefit state, provincial,
159 and federal natural resource agencies and non-governmental agencies in generating survival,
160 distribution, population, and carrying capacity projections for wildlife influenced by winter
161 severity. To date, a lack of quality 21st century snow projections has hindered the capacity to
162 estimate the potential effects of climate change on species which are sensitive to snowpack and
163 temperature, such as white-tailed deer and dabbling ducks.

164

165 **2. Data and Methods**

166 *2.1 Statistical downscaling*

167 Through the Wisconsin Initiative on Climate Change Impacts (WICCI), a daily
168 statistically downscaled climate projection product was developed to guide climate change
169 impact and adaptation studies (WICCI 2011). Notaro et al. (2011) used this downscaled data to
170 force an operational snow model, SNOW-17, and generate high-resolution snow projections for
171 Wisconsin. The current study uses an improved version of the downscaling covering the United
172 States and southern Canada, namely ten of the LCCs to the east of the Rocky Mountains (Tables
173 1-2), at $0.1^\circ \times 0.1^\circ$ resolution. The downscaled variables are daily maximum temperature,
174 minimum temperature, and precipitation for the late 20th (1961-2000), mid-21st (2046-2065), and
175 late 21st centuries (2081-2100), based on three CMIP3 emission scenarios (A2, A1B, B1) and 13
176 GCMs. The present study focuses on the 9 GCMs (Table 3) for which downscaled projections
177 are available for the late 20th century (20C3M) and each emission scenario, with results shown
178 for the contrasting high-end (A2) and low-end (B1) scenarios. By the year 2100, atmospheric
179 carbon dioxide levels are projected to reach 840 and 550 ppm, under the respective scenarios.

180 The station data used to train the statistical models consists of daily maximum and
181 minimum temperature and precipitation from the National Weather Service's (NWS)
182 Cooperative Observer Program (1950-2009) and Environment Canada's Canadian Daily Climate
183 Data (1950-2007), for roughly 4000 stations in the United States and Canada. Objective
184 methods are applied to correct the hour of observation and remove stations with large biases in
185 wet day frequency (Daly et al. 2007). Only stations with at least 30 years of data, and fewer than
186 five missing days per month, are included. The large-scale atmospheric state is obtained the

187 National Centers for Environmental Prediction (NCEP)-NCAR Reanalysis (Kalnay et al. 1996).
188 The downscaling methodology is probabilistic, as a given large-scale state does not determine a
189 single, precise value for a location's temperature or precipitation, but rather the parameters'
190 values in a parametric probability density function (PDF). These PDF parameters vary daily
191 with the large-scale fields. A normal distribution is used for maximum and minimum
192 temperature, a generalized gamma distribution (Stacy 1962) is used for precipitation amount on
193 wet days, and the probability of measurable precipitation is modeled with logistic regression. A
194 realistic temperature skewness is simulated, because the final temperature distribution is
195 determined by both the large-scale predictors and normally-distributed noise added to the mean.
196 Unlike classic linear regression, the variance is allowed to change, based on large-scale fields.

197 The reanalysis predictors for daily maximum (minimum) temperature include the 2-m
198 maximum (minimum) temperature itself, 1000-m wind vector, and column-integrated relative
199 humidity. Here, column-integrated relative humidity is a measure of the lower to mid-
200 tropospheric water holding capacity, computed as the ratio of the sum of specific humidity
201 between sigma levels 0.9 and 0.5 and the sum of the saturated specific humidity between those
202 levels. For the probability of measurable precipitation, the predictors are precipitation rate to the
203 0.25 power, column-integrated relative humidity, average wind vector between sigma levels 0.9
204 and 0.5, and a pseudo-K index. The inclusion of wind as a predictor allows for the
205 representation of lake-effect precipitation. The K index is defined as:

$$K = T_{850\text{hPa}} - T_{500\text{hPa}} + TD_{850\text{hPa}} - (T_{700\text{hPa}} - TD_{700\text{hPa}}) \quad (2)$$

206 where T is temperature and TD is dew point, both in °C. Given that the K index equation
207 contains an imbalance of three temperature values and two dew point values, a projected increase
208 in temperature would almost certainly imply increased instability, which may or may not be

realistic. If relative humidity is constant, which is a reasonable first-order approximation for global warming, then both the dew point temperature and actual temperature increase by the same amount. Therefore, the pseudo-K index is computed by eliminating the $T_{850\text{hPa}}$ term. To make the index suitable for high elevations, sigma levels are used. The pseudo-K index is defined as:

$$K_{\text{pseudo}} = -T_{0.5\sigma} + TD_{0.9\sigma} - (T_{0.7\sigma} - TD_{0.7\sigma}). \quad (3)$$

The predictors for precipitation amount include precipitation itself, the pseudo-K index, available water, and available water flux. The latter two predictors are motivated by the scaling relationships between moisture and precipitation under climate change (O’Gorman and Schneider 2009). The available water is defined as the amount of water that is condensed out when an air parcel is lifted vertically from its current pressure to half its pressure. Using the wind field, the available moisture flux is computed. The available water and available water fluxes are averaged vertically between sigma levels 0.9 and 0.5 before serving as predictors.

The above statistical models determine the spatially and temporally varying PDFs of maximum and minimum temperature and precipitation at each station and day in the observed record. To apply the downscaling to climate models, the cumulative distribution function remapping algorithm of Wood et al (2004) is used to debias the GCM predictors to match the reanalysis. The statistical models are then applied to the debiased model predictors, creating downscaled PDFs for each station and day in the climate models.

To create a gridded downscaling dataset, the PDF parameters are interpolated to a predefined grid. In the study by Notaro et al. (2011), the PDFs were interpolated to a grid based on distance to surrounding stations. The mean temperature at a grid point, g , was given by:

$$T(g) = \sum_j \exp(-(d(g, s_j)/D)^2), \quad (4)$$

233 where the summation is across stations, $d(g, s_j)$ is the distance between the grid point and station,
 234 s_j , and D is a parameter that is fit by leaving each station out in turn and using (4) to predict the
 235 station's temperature from the remaining stations. The D that minimizes the error over all
 236 stations was used. A different value of D was found for each variable and month. In the new
 237 downscaling, (4) is modified, so that the weighting also depends on the difference in the mean
 238 climate between the stations, s_j , and the grid point:

$$239 \quad T(g) = \sum_j \exp\left(-(d(g, s_j)/D_1)^2 - |\Delta T(g, s_j)|/D_2\right), \quad (5)$$

240 where $\Delta T(g, s_j)$ is the mean temperature difference between the grid point and the station. The
 241 mean climate is obtained from the Parameter-elevation Regressions on Independent Slopes
 242 Model (PRISM) (Daly 2006; Daly et al. 2008) and the Canadian Normals dataset (McKenney et
 243 al. 2001). These datasets are interpolated to the downscaling grid and to the stations using
 244 bilinear interpolation. Using PRISM and the Canadian Normals dataset adds information
 245 because the fitting of the conditional PDF estimates requires stations with extensive data, while
 246 the PRISM and Canadian Normals data are intended only to estimate the mean. Therefore, many
 247 more stations are used to constrain the mean climate in the PRISM and Canadian Normals
 248 datasets. In addition, PRISM estimates the role of topography and proximity to coastlines in its
 249 interpolation scheme. In (5), the mean climate effect is intentionally of lower order than the
 250 distance term, so that the distance term dominates if one is far removed from the grid point.
 251 Stations with a similar climate are given extra weight only if they are relatively close to the grid
 252 point. The constants, D_1 and D_2 , are found by cross validating over stations.

253 In regions of complex topography and data sparse regions of Canada, the downscaling is
 254 relatively unconstrained by data, as the applied approach is restricted to stations with long
 255 records. Therefore, PRISM and the Canadian Normals dataset are also used to adjust the mean

maximum and minimum temperature and precipitation. For temperature, an additive correction is used, which is the difference between the PRISM/Canadian Normals dataset and gridded downscaled data. For precipitation, a multiplicative correction is used. This correction is not meant to correct the downscaled mean of the station data. For example, the conditional mean for temperature is determined by ordinary least squares regression, so the mean is exact to numerical precision. Instead, this correction is used to provide additional information in between stations in regions of complex topography and in data sparse regions, as confirmed by the fact that the corrections are small, except in mountains and parts of Canada.

Spatially and temporally varying PDFs of maximum/minimum temperature and precipitation are now known at each grid and day. To generate normal data, random numbers are drawn from the PDFs, generating a possible realization of the small-scale state that is consistent with the large-scale fields. The random numbers are correlated in space (and time, in the case of temperature) so that the spatial and temporal correlations of the downscaled variables are similar to observations. One of the randomly-generated realizations is used to drive the snow model.

To help gauge the fidelity of the downscaling, temperature and precipitation variability and the co-variability between temperature and precipitation are compared between the observations and downscaled data for winter. The downscaling, by design, reproduces the mean climate, so this analysis does not focus on the mean. All variables are averaged across the nine climate models before plotting the results. For the standard deviation in daily maximum temperature (Supp. Fig. 1a,b), the downscaling reproduces the strong variability from the Great Plains to the Ohio Valley and weak variability near the Great Lakes and coasts. The largest errors are found in Florida, where the downscaled maximum temperature variability is too large. For the standard deviation in daily minimum temperature (Supp. Fig. 1c,d), the downscaling

279 reproduces the strong variability in the north and relatively weak variability near the Great Lakes,
280 Atlantic coast, and southwestern Great Plains.

281 Given that projected snowfall extremes are examined in this study, precipitation extremes
282 in the observations and downscaling data are compared (Supp. Fig. 2). The downscaled
283 extremes are calculated directly from the PDFs and thus exhibit less sampling variability (spatial
284 noise) than the observations. The downscaling reproduces the spatial patterns and magnitudes of
285 the observed 99.9th and 99.99th percentiles. The largest differences are found across the
286 Southeast United States for the 99.99th percentile, although given the limited sample size, a
287 significant portion of the differences likely results from sampling variability.

288 The correlation between daily wintertime temperature and precipitation is assessed (Supp.
289 Fig. 3). Unlike the precipitation and temperature variability, no attempt was made to fit the
290 correlation between temperature and precipitation. The correlations in the downscaling are those
291 that naturally appear as a result of co-variability in the large-scale predictors used to individually
292 predict temperature and precipitation. For maximum temperature and precipitation, the
293 downscaling reproduces the general pattern of positive correlations in the Northeast and negative
294 correlations in the western Great Plains. The downscaling also shows decreased correlations to
295 the lee of the Appalachians, although the downscaled correlations are too positive. The
296 downscaled correlations tend to be too large across the Northeast. For minimum temperature
297 and precipitation, the downscaling reproduces the general large-scale patterns, although the
298 downscaled correlations are too large across the northwest Great Plains and around Tennessee.

299

300 *2.2 Snow model*

301 SNOW-17 is an empirically-based, operational snow accumulation and ablation model
302 (Anderson 1973, 2002, 2006; Franz et al. 2012a,b; Raleigh and Lundquist 2012), a component of
303 the NWS River Forecast System. SNOW-17 treats the key physical processes that regulate snow
304 dynamics in a conceptual manner, requiring only commonly available data observations of
305 temperature and precipitation as inputs (Supp. Fig. 4). In treating a column of snowpack, the
306 model addresses the following principal processes: form of precipitation, snow accumulation,
307 energy exchange at the snow-air interface, heat exchange at the soil-snow interface, heat storage
308 and deficit within the snowpack, and liquid water retention and transmission of water through the
309 snow cover (Anderson 2006). Snow cover is modeled as a single, bulk layer with a specified
310 water holding capacity. The density of new snow is treated as a function of air temperature,
311 while the density of existing snow responds to compaction, destructive metamorphism, and the
312 component of melt metamorphism due to the presence of liquid water (Anderson 2006). The
313 simple temperature-based SNOW-17 model performs at least as well as more physically-based
314 energy balance models (Anderson 1973, 1976; Ohmura 2001; Zappa et al. 2003; Franz et al.
315 2008a). There is a precedent to applying SNOW-17 in climate change studies (Notaro et al.
316 2011). Prior studies have used either SNOW-17, or the Sacramento Soil Moisture Accounting
317 Model (Burnash et al. 1973) coupled to SNOW-17, forced by climate projection data, to
318 investigate potential changes in California water resources and reservoir operations (Miller et al.
319 2003; Brekke et al. 2009; Maurer et al. 2010; Hanson et al. 2012).

320

321 *2.3 Datasets*

322 Hourly air temperature data at 12 weather stations across the United States for 1980-1999
323 is used to compute their mean diurnal cycle for DJF and identify the times of maximum and

minimum temperature. The station data is extracted from the National Climatic Data Center (NCDC) Global and U.S. Integrated Surface Hourly dataset (<http://www.ncdc.noaa.gov/cdo-web>) for Billings, MT; Havre, MT; Pueblo, CO; and Cheyenne, WY in the western study region (103-116°W), LaCrosse, WI; Dubuque, IA; Madison, WI; and Oklahoma City, OK in the central region (87-103°W), and Bangor, ME; Atlanta, GA; Greenville, SC; and Teterboro, NJ in the eastern region (67-87°W). Based on these stations, it is determined that the daily minimum and maximum temperatures in DJF typically occur at 14Z (range: 14-15Z) and 22Z (20-22Z) in the western region, 13Z (11-14Z) and 21Z (20-21Z) in the central region, and 12Z (10-12Z) and 20Z (19-21Z) in the eastern region, respectively. This information aids the interpolation of downscaled daily maximum and minimum temperatures to hourly values, for input to SNOW-17.

Based on hourly present weather (rain or snow occurrence) and air temperature for 1980-1999 at 135 stations across the study region, from the NCDC Global and U.S. Integrated Surface Hourly dataset, the mean snow-rain temperature threshold is computed at different locations and assigned to the SNOW-17 parameter, PXTEMP. Climatologies of snow depth and surface soil temperature for DJF from the North American Regional Reanalysis (Mesinger et al. 2006) are used to estimate SNOW-17's antecedent temperature index parameter (TIPM) and the parameter for daily snowmelt at the snow-soil interface (DAYGM), respectively. The SI parameter, which quantifies the required amount of liquid snow for 100% cover, is determined by applying values used by the Noah Land Surface Model to an International Geosphere-Biosphere Programme Land Cover map. Detailed descriptions of SNOW-17 parameters are provided in the Supplemental Materials. Annual snowfall and snow depth climatologies for 1981-2000 are computed for a different set of 196 stations across the study region from NCDC Local Climatological Data Publications (<http://www.ncdc.noaa.gov/IPS/lcd/lcd.html>) and Environment

347 Canada's Canadian Climate Normals (http://climate.weather.gc.ca/climate_normals) and used to
348 tune and evaluate SNOW-17. Elevation is retrieved from the ETOP02 Gridded Global Relief
349 Data (National Geophysical Data Center 2013).

350

351 *2.4 SNOW-17 simulations and their evaluation*

352 After calibrating SNOW-17 and its parameters across the study region, the model is run
353 for the late 20th century (1981-2000), mid-21st century (2046-2065), and late 21st century (2081-
354 2100), according to the A2 and B1 emission scenarios. For each time period, statistically
355 downscaled climate data from nine CMIP3 GCMs is used to force the snow model across the ten
356 LCC regions of central-eastern North America (Fig. 1). SNOW-17 generally requires hourly
357 climatic inputs. Downscaled daily maximum and minimum temperature is converted to hourly
358 temperature data using an interpolatory cubic spline under tension, with the minimum and
359 maximum temperature assigned to 12-14Z and 20-22Z, respectively (depending on longitude).
360 This interpolation approach of converting daily maximum and minimum temperatures into
361 hourly temperatures is successful in maintaining different projected changes in maximum versus
362 minimum temperature, recognizing that most GCMs simulate a greater increase in minimum
363 temperature. Daily precipitation amounts are converted into hourly values by randomly
364 distributing the precipitation on wet days into continuous six-hour periods (0-6Z, 6-12Z, 12-18Z,
365 or 18-24Z), which is the typical duration of a cold-season precipitation event based on studies for
366 the Midwest and Northeast United States (Cox and Armington 1914; Changnon 1969; Knapp et
367 al. 2000; Laird et al. 2009).

368 SNOW-17 requires regionally-specific calibration to produce quality snow simulations.
369 The model applies six major parameters (SCF, MFMAX, MFMIN, UADJ, SI, and ADC) and six

370 minor parameters (MBASE, NMF, DAYGM, PLWHC, PXTEMP, and TIPM). The
371 methodology for determining appropriate parameter values is outlined in the Supplemental
372 Materials. The model is tuned to best capture climatological patterns of annual snowfall and DJF
373 snow depth, compared to observations at 196 stations (Fig. 1).

374 Using the resulting parameter values, SNOW-17 is forced by statistically downscaled
375 climate data from nine CMIP3 GCMs for 1981-2000. The simulated climatological patterns of
376 annual snowfall and DJF snow depth (averaged among nine GCMs) are evaluated against the set
377 of 196 stations (Fig. 2). The observed and simulated mean annual snowfall closely match, with a
378 correlation of 0.99 (ranging from 0.95 in April to 0.99 in December/January), root-mean-square-
379 difference of 5.9 cm (ranging from 2.8 cm in November to 3.4 cm in December), and a mean
380 absolute difference of 3.8 cm. Due to biases in selected parameter values, the model produces
381 excessive snowfall in December-January (+8.3% in December) and too little in November and
382 February-April (-14.8% in November). Regarding DJF climatological snow depth, the model
383 and observations exhibit slightly less agreement, with a correlation of 0.90 (ranging from 0.86 in
384 March to 0.95 in November), root-mean-square-difference of 4.4 cm (ranging from 0.4 cm in
385 November to 6.7 cm in February), and a mean absolute difference of 1.3 cm. The simulated
386 snowpack is too deep in spring, due to insufficient snowmelt. Percent biases range from -7% in
387 November to +37% in March. Overall, SNOW-17 performs quite well in reproducing the
388 modern-day snow climatology across the vast study region when forced with statistically
389 downscaled climate data, with a distinct improvement over the original GCMs (Supp. Fig. 7).

390

391 **3. Results**

392 *3.1 Downscaled climate projections*

393 At every location in the study region, and according to both emission scenarios, warming
394 is a robust projection for DJFM by the mid- and late 21st century by all nine downscaled GCMs.
395 According to the B1 and A2 scenarios, the area-average increase in surface air temperature by
396 the mid-21st century is +2.0°C (range: +1.3°C to +2.6°C) and +2.9°C (+2.0°C to +4.3°C) and by
397 the late 21st century is +3.1°C (+2.1°C to +4.2 °C) and +5.3°C (+4.1°C to +6.2°C), respectively
398 (Fig. 3). The scenarios diverge by the late 21st century in terms of the magnitude of projected
399 warming. The degree of warming increases with latitude and displays a local minimum in the
400 Great Lakes Basin. The greatest mean projected warming by the late 21st century, from the A2
401 scenario, is found across the Upper Midwest and Great Lakes LCC (+6.0°C) and Plains and
402 Prairie Potholes LCC (+5.7°C) (Tables 1-2; Fig. 3). In this study, at each grid cell, the “low-end
403 projection” and “high-end projection” in temperature refer to the least and most warming,
404 respectively, among the nine downscaled GCMs. The A2-based low-end and high-end
405 projections by the late 21st century differ dramatically by roughly 3.5-4°C across Michigan and
406 southern Canada (Fig. 3a,c,d), indicating consistent projections of warming but much uncertainty
407 regarding its magnitude (particularly in minimum temperatures). This uncertainty may be
408 attributed to: (1) greater natural variability with increased latitude, (2) variations in the intensity
409 of snow-ice feedbacks among GCMs, and (3) differing representations of the Great Lakes among
410 the original GCMs (e.g. GCMs excluding the lakes may warm more regionally).

411 There is even greater uncertainty in DJFM projections of precipitation than temperature
412 among GCMs. The area-average projected change in DJFM precipitation by the mid-21st
413 century is +0.09 mm/day (range: -0.01 to +0.21 mm/day), or +5.3%, according to the B1
414 scenario and +0.13 mm/day (+0.03 to +0.25 mm/day), or +7.4%, according to the A2 scenario
415 (Fig. 4); projections for the late 21st century are +0.13 mm/day (-0.01 to +0.31 mm/day), or

416 +7.4%, for the B1 scenario and +0.20 mm/day (+0.00 to +0.32 mm/day), or +11.5%, for the A2
417 scenario. The model-mean DJFM projections for the late 21st century, based on the A2 scenario,
418 range from -0.19 mm/day (-10.7%) in the Gulf Coast Prairie LCC to +0.61 mm/day (+21.7%) in
419 the North Atlantic LCC, with the largest increases over the Northeast United States (Fig. 4b,
420 Tables 1-2). Precipitation projections largely disagree among the GCMs across the Gulf Coastal
421 Plains and Ozarks LCC, ranging from drying of about -1 mm/day to moistening of about +1.0
422 mm/day (Fig. 4a,c,d). While a potential decline in precipitation across the southern LCCs would
423 reinforce the effect of warming to reduce snowfall, a robust projection of greater precipitation
424 across the northernmost LCCs should counter the impact of warming on future snowfall.

425

426 *3.2 Benefits of downscaling for snow simulations*

427 Given the coarse horizontal resolution of the CMIP3 GCMs (mean grid cell size of
428 7.4×10^4 km²) and insufficient representation of the Great Lakes (either completely absent or
429 represented by a few grid cells), lake-effect processes are largely neglected; unfortunately, this
430 limitation continues to exist in most CMIP5 GCMs. However, by including wind as a
431 precipitation predictor in the statistical downscaling, lake-effect precipitation events are captured
432 in the downscaling product, and therefore SNOW-17 simulations forced by this downscaled data
433 include lake-effect snowstorms. To illustrate this point, two December days are selected from
434 the GISS Model E-R and MPI ECHAM5, with cold air outbreaks and associated west-
435 northwesterly low-level winds over the lakes at a time of the year when ice cover is usually
436 limited and therefore lake-effect snow would be supported (Fig. 5a,b). However, in both cases,
437 there is no signature of lake-effect precipitation in the GCM (Fig. 5a,b). SNOW-17, when forced
438 by the statistical downscaling data, produces distinct lake-effect snowfall maxima downwind of

439 the lakes on both days (Fig. 5c,d). Clearly, the downscaling relies on the strength of GCMs,
440 which is the representation of large-scale circulation patterns, and adds accuracy to the
441 projections by relating the GCM's large-scale circulation patterns to the expected local climatic
442 response, as established through the observations.

443 Compared to the raw GCMs, the use of statistically downscaled climate data in SNOW-
444 17 results in a more reasonable spatial pattern of annual mean climatological snowfall across the
445 study region. The mean observed snowfall peaks across the Northeast United States, southern
446 Ontario-Quebec, the Great Lakes Basin, Appalachian Mountains, and on the lee side of the
447 Rocky Mountains (Figs. 2, 6c). The mean snowfall climatology among the raw CMIP3 models
448 crudely captures this spatial pattern but contains significant biases and minimal signature of the
449 Great Lakes or Appalachian Mountains (Fig. 6a). However, when forced by downscaled climate
450 data, SNOW-17 produces minimal biases in annual snowfall and accurately represent the lake-
451 effect snow maxima and elevated snowfall over the Appalachian Mountains (Fig. 6b). For the
452 comparisons in Fig. 6 and Supp. Fig. 7, given that the GCMs only saved liquid-equivalent of
453 snowfall, a 10:1 ratio is applied to crudely convert the liquid-equivalent snowfall to simulated
454 snowfall depth. Krasting et al. (2013) likewise applied a 10:1 ratio to the CMIP3 snowfall mass
455 flux output but cautioned that this ratio has significant observed regional variations. The lake-
456 effect zones of the Great Lakes Basin are typically characterized by greater snow-to-liquid-
457 equivalent ratios of 14:1 or 15:1 (Baxter 2005; Kutikoff 2013).

458

459 *3.3 Snow projections*

460 The model-mean projections, for both emission scenarios and both time periods, indicate
461 a warming-induced decline in annual snowfall across the entire study region (Fig. 7b,e,h,k). The

462 area-average mean projections for annual snowfall, by the mid-21st century, are -17.9 cm (range:
463 -8.4 to -28.6 cm), or -16.6%, according to the B1 scenario and -26.0 cm (-19.0 to -37.8 cm), or -
464 24.2%, according to the A2 scenario (Fig. 7); these projections for the late 21st century are -28.4
465 cm (-14.6 to -35.9 cm), or -26.4%, for the B1 scenario and -45.0 cm (-32.5 to -55.7 cm), or -
466 41.8%, for the A2 scenario. The largest declines, by the late 21st century, are projected for the
467 North Atlantic LCC (-58.8 cm, or -30.8%, for B1 versus -92.0 cm, or -48.1%, for A2) and the
468 Upper Midwest and Great Lakes LCC (-53.9 cm, or -24.1%, for B1 versus -89.9 cm, or -40.2%,
469 for A2) (Tables 1-2), as precipitation falls more in the form of rain than snow. By the late 21st
470 century, the two emission scenarios result in similar patterns of projected snowfall decline,
471 although the high-end projection (defines as the largest decline) for A2 produces about 25%
472 greater snowfall declines across the domain than does B1 (Fig. 7f,l). According to the low-end
473 projection (smallest decline, or a potential increase) for annual snowfall, relatively modest
474 increases are possible across southern Canada and the Plains and Prairies Potholes LCC, and the
475 southern states, as increases in cold season precipitation offset the warming trend (Fig. 7a,d,g,j).

476 The mean frequency of snowfall days, in excess of 1 cm, is projected to decline at every
477 grid cell by the mid- and late 21st century, according to model-mean results from both emission
478 scenarios (Fig. 8a-d). During the late 20th century, SNOW-17 simulates a mean frequency of
479 snowfall days that ranges from 0.01 day in the Peninsular Florida LCC to 39.08 days in the
480 Upper Midwest and Great Lakes LCC. The largest model-mean declines in snowfall days are
481 projected for the Upper Midwest and Great Lakes LCC (B1: mean = -8.9 days, or -22.9%, range
482 = -2.6 to -13.8 days; A2: mean = -15.6 days, or -39.9%, range = -12.2 to -19.6 days) and the
483 North Atlantic LCC (B1: mean = -8.2 days, or -28.2%, range = -4.4 to -11.8 days; A2: mean = -
484 13.7 days, or -46.7%, range = -8.6 to -18.0 days) (Tables 1-2, Fig. 8a-d). According to the B1

485 scenario, a modest increase in the frequency of snowfall days by the mid-21st century is
486 identified across northern Wisconsin, Minnesota, and Montana for the low-end projection
487 (defined as the smallest decline, or greater increase, in snowfall days among the nine GCMs).

488 Despite large projected declines in annual-mean snowfall and snowfall frequency across
489 the study region, SNOW-17 produces only slight changes in mean snowfall intensity, or total
490 daily snowfall per event (Fig. 8e-h). Most areas are simulated to experience lighter snowfall
491 events, with declines in mean snowfall intensity simulated across 64% of the study region by the
492 mid-21st century with the B1 scenario, and across 79% of the region by the late 21st century with
493 the A2 scenario (Fig. 8e-h). However, an increase in snowfall intensity is possible for southern
494 Canada and the Gulf states (Fig. 8e-h). Results from Figs. 7-8 for southern Canada imply lower
495 annual snowfall totals, fewer snowfall days, and higher snowfall totals per event, which suggest
496 fewer, but more intense, snowfall events. Model-mean projections for snowfall totals per event,
497 by the late 21st century, are modest and differ notably across models. Projected intensity changes
498 for the Great Plains LCC are -0.26 cm (range: -1.00 to +0.54 cm), or -4.1%, for the B1 scenario
499 and -0.52 cm (-1.29 to +0.24 cm), or -8.4%, for the A2 scenario (Tables 1-2). For the Gulf
500 Coastal Plains and Ozarks LCC, these projections include +0.10 cm (range: -0.58 to +1.24 cm),
501 or +2.2%, for the B1 scenario and -0.62 cm (-1.37 to +0.03 cm), or -14.3%, for the A2 scenario;
502 in this region, snowfall events are rare, making these conclusions uncertain.

503 Projected percentage changes in the frequency of snowfall events of different daily
504 magnitudes are computed both across the study region and within individual LCC regions (Fig.
505 9). For both scenarios and time periods, the projected percentage reduction in the frequency of
506 daily snowfall events is maximized around 15-23 cm, ranging from -21.5% by the mid-21st
507 century under the B1 scenario to -47.6% by the late 21st century under the A2 scenario (Fig. 9).

508 Consistent with GCM projections for heavier precipitation events later this century, SNOW-17
509 simulates more frequent intense snowfall events, particularly by the mid-21st century, under the
510 low-end emission scenario (B1), and across the north-northwest study region. Specifically, daily
511 snowfall events exceeding (under) 70 cm are projected to become more (less) frequent across the
512 study region by the mid-21st century, for the B1 scenario (Fig. 9). Under more extreme warming
513 projections (late 21st century or A2), the potential for heavier snowfall events diminishes
514 substantially (Fig. 9). The projected increase in frequency of heavy daily snow events is
515 primarily confined to the Plains and Prairie Potholes LCC and Upper Midwest and Great Lakes
516 LCC (Fig. 9), for events exceeding 56 cm for the mid-21st century and B1 scenario or 76 cm for
517 the late 21st century and A2 scenario.

518 With larger projected snowfall declines in autumn than spring, SNOW-17 generally
519 simulates a delayed onset of the snow season, more prominently than an earlier termination (Fig.
520 10). During the cold season (November-April), the study region is projected to warm the most
521 during November-December, with the largest reductions in snowfall during December-January,
522 as evident for the late 21st century and A2 scenario in Fig. 10. The primary exception is found
523 across the northern Great Plains, particularly South Dakota, Nebraska, Colorado, and Wyoming,
524 with the greatest projected decline in snowfall during springtime (March-April); these regions
525 are characterized by high rain-snow temperature thresholds exceeding 1.5°C (Supp. Fig. 5a).

526 For all 10 LCC regions, the projected percentage reduction in mean November-April
527 snow depth exceeds that of snowfall, as projected warming also accelerates snow melt. For
528 example, the North Atlantic LCC is expected to experience a 48.1% reduction in annual snowfall
529 and a 72.1% reduction in November-April snow depth, by the late 21st century according to the
530 A2 scenario (Tables 1-2, Fig. 11). The largest projected reductions in snow depth are found

531 within the Upper Midwest and Great Lakes LCC, with decline by the late 21st century of -7.63
532 cm (-36.9%) for the B1 scenario versus -11.94 cm (-57.8%) for the A2 scenario. Across the
533 study region, November-April mean snow depth is projected to decline by -1.79 cm (range: -1.12
534 to -2.67 cm) according to the B1 scenario and -2.56 cm (range: -1.95 to -3.30 cm) according to
535 the A2 scenario, by the mid-21st century; late 21st century projections include declines of -2.72
536 cm (range: -1.50 to -4.08 cm) for the B1 scenario and -4.11 cm (range: -3.17 to -4.78 cm) for the
537 A2 scenario. Here, the snow line, or southernmost mean extent of snow cover in a region, is
538 defined by a criterion of at least 0.5 cm of mean snow depth during November-April. The snow
539 line across the study region is anticipated to shift northward by 72 km (128 km) by the mid-21st
540 century and 126 km (229 km), according to the B1 (A2) scenario. The projected northward
541 migration rate of the snow line is less than half of that of the mean isotherms during DJFM (for -
542 5°C to 5°C), implying a more gradual response to climate change. The low-end projection
543 among the nine GCMs suggests the potential for a slight increase in annual mean snowfall and
544 snow depth across the southern states, with a large percentage increase (Fig. 11 a,d,g,j).

545 Projected changes in the annual number of days with a minimum snowpack of 1 cm are
546 assessed (Fig. 12). The regions likely to experience the largest reductions in days with snowpack
547 are the Upper Midwest and Great Lakes LCC, North Atlantic LCC, and Plains and Prairie
548 Potholes LCC, with respective decline of -27.0 days (-19.7%, range: -16.2 to -42.8 days), -28.5
549 days (-30.3%, -18.3 to -36.7 days), and -26.3 days (-22.2%, -17.1 to -47.2 days) for the B1
550 scenario and -47.6 days (-34.8%, -35.7 to -62.0 days), -47.3 days (-50.3%, -31.8 to -60.0 days),
551 and -42.7 days (-35.9%, -29.5 to -55.9 days) for the A2 scenario (Tables 1-2). An optimal zone
552 of maximum reduction in days with snowpack is identified near 44°N, closely following the -5°C
553 isotherm of the late 20th century mean climatology (Fig. 12). As this isotherm shifts northward

554 during the 21st century, trends in declining snowfall accelerate. Ratios between the projected
555 snowfall decline by the late 21st century and the projected decline by the mid-21st century are on
556 the order of 1.4-1.6 (e.g. 1.46 in the South Atlantic LCC) to the south of this isotherm and 1.6-
557 2.0 to the north (e.g. 1.67 in the Upper Midwest and Great Lakes LCC) (Fig. 13). The northern
558 LCCs can expect an accelerated negative trend in annual snowfall during this century.

559

560 *3.4 Application of SNOW-17 projections for predicting wintertime waterfowl distributions*

561 To illustrate the utility of these SNOW-17 based projections, dabbling ducks are selected
562 for a case study, with the focus on the CWSI of Schummer et al. (2010), which addresses their
563 energetics and food requirements. CWSI is computed for the late 20th, mid-21st, and late 21st
564 centuries, according to the A2 and B1 scenarios (Tables 1-2, Fig. 14). Here, analysis is focused
565 on the CWSI=7.2 isopleth, which is the threshold at which mallards are predicted to decrease in
566 abundance (i.e., increasing likelihood of southward migration) (Schummer et al. 2010), thereby
567 providing an index of relative duck distribution. During Januaries in the late 20th century, this
568 isopleth was typically located across central Kansas, southern Illinois, and southern Ohio (Fig.
569 14j). In response to projected warming and declining snowpack, this isopleth is expected to shift
570 northward; under the A2 scenario, it is projected in January to be positioned across northern
571 Nebraska, northern Illinois, and central Michigan by the late 21st century. In general, the arrival
572 of this isopleth from Canada into the United States could be delayed by roughly one month in
573 late autumn, by the late 21st century. The largest reductions in mean DJF CWSI are expected for
574 the Upper Midwest and Great Lakes LCC, from 94.9 during the late 20th century to either 60.5 or
575 40.3, for the B1 and A2 scenarios, respectively (Tables 1-2). Within the study region, the
576 probability of WSI>7.2 (i.e., likelihood of mallards' southward migration) is projected to decline

577 most substantially during December across the northern LCCs (e.g. Plains and Prairie Potholes)
578 and during January across the central LCCs (e.g. Eastern Tallgrass Prairie and Big Rivers) (Fig.
579 14). For example, during Decembers in the late 20th century, there was a 62.5% probability of
580 WSI>7.2 across the North Atlantic LCC. By the late 21st century, this probability is projected to
581 decrease to 40.4% for the B1 scenario or 19.8% for the A2 scenario (Fig. 14f), suggesting that
582 mallards might delay their southward migration during early winter.

583

584 4. Discussion and Conclusions

585 High-resolution projections of daily snowfall, snow depth, and winter severity for the
586 mid-21st and late 21st century are generated for the central-eastern North American LCCs. A
587 snow accumulation and ablation model, SNOW-17, is forced with statistically downscaled
588 climate data from nine CMIP3 GCMs and two emission scenarios. These cold season
589 projections will aid natural resource agencies in assessing impacts of changes in snow and winter
590 severity to wildlife. Compared to raw GCM snow output, this approach leads to a better
591 representation of weather extremes, lake-effect processes (by including wind as a downscaling
592 predictor), and topographic influences, along with smaller biases in snowfall and snow depth.

593 For both time periods and both emission scenarios, the entire study region is expected to
594 experience a reduction in annual snowfall and shift towards less snow and more rain, based on
595 model-mean projections. The largest snowfall losses are simulated for the North Atlantic LCC
596 and the Upper Midwest and Great Lakes LCC, with respective declines by the late 21st century of
597 -48.1% and -40.2% under the A2 scenario. For much of the region, snowfall is projected to
598 decline the most during December-January, implying a delayed onset of the snow season, except
599 over the Northern Plains, where the greatest losses are expected in March-April when

600 snowstorms are more common (Changnon et al. 2006). These results are consistent with studies
601 by Kapnick and Delworth (2013) and Krasting et al. (2013), which project a general decline in
602 Northern Hemispheric snowfall, including across North America, outside of the high latitudes.
603 Considering the range of outcomes from nine GCMs for the B1 scenario, there is a potential for
604 an increase in annual snowfall across southern Canada, north of the historical mean position of
605 the -10°C isotherm in DJFM, by both the mid- and late 21st century, in response to greater
606 precipitation. Similarly, Krasting et al. (2013) concluded that snowfall would increase to the
607 north of that same isotherm and decrease to the south. SNOW-17 simulates a trend towards
608 fewer snowfall days, but with modest changes in mean intensity. A larger percentage decline in
609 mean snow depth is simulated than in annual snowfall, due to enhanced snowmelt rates with
610 warming. The mean snow line is simulated to shift northward, ranging from 72 km by the mid-
611 21st century according to the B1 scenario to 229 km by the late 21st century according to the A2
612 scenario. The projected decline in the number of days with a present snowpack is expected to
613 optimally peak around 44°N, close to the mean -5°C DJFM isotherm. Dramatic decreases are
614 simulated in both mean CWSI and the probability of CWSI exceeding 7.2, which is the critical
615 threshold for mallard duck migration. The arrival of this critical WSI isopleth from Canada into
616 the United States may become delayed about a month by the late 21st century, delaying the ducks'
617 southward migration in early winter.

618 A diminished snowpack across central-eastern North America will substantially impact
619 terrestrial ecosystems, wildlife, and society. A shift in snowmelt from spring to winter (Manabe
620 et al. 1981; Mahanama et al. 2011) will favor diminished spring-summer soil moisture (Mastin et
621 al. 2011) and greater summertime droughts (Mishra et al. 2010; Mahanama et al. 2011). The
622 winter recreational industries and tourism will experience large economic losses (Scott et al.

623 2008). Milder conditions and diminished snowpack will increase the mobility and decrease the
624 mortality rates of white-tailed deer (Severinghaus 1947; Edwards 1956; Verme 1968), while
625 increasing risk to animals that depend on winter camouflage.

626 Projected decreases in CWSI suggest substantial changes to the migratory behavior and
627 distributions of waterfowl. Duck watching and hunting are major sources of recreation and
628 revenue. The southward movement of waterfowl each year enables millions of people to
629 participate in these activities. In 2011 alone, roughly 2.6 million migratory bird hunters in the
630 United States generated \$3.4 billion in revenue (U.S. Fish and Wildlife 2011; Southwick
631 Associates 2012). North American waterfowl number in the millions, use a diversity of aquatic
632 and terrestrial foraging niches, and can feed at rates capable of depleting local food resources.
633 Recently, waterfowl appear to be wintering at more northern latitudes (Abraham et al. 2005;
634 Link et al. 2006; Svažas et al. 2001). Sustained northern shifts in autumn-winter distributions of
635 abundant waterfowl could increase foraging pressure at the Great Lakes. The loss of migrating
636 waterfowl in the Deep South would induce sizable economic losses to rural America tied to
637 wildlife-based recreation (Grado et al. 2011).

638 Few studies have addressed the impact of future climate change on the frequency of
639 heavy snow events (Gutowski et al. 2008; López-Moreno et al. 2011). Changnon (2007) found
640 that 88% of the economic losses attributed to United States' snowstorms during 1949-2003
641 occurred in the eastern half of the country. Snowstorms in the United States have become less
642 frequent, but larger and more intense (Changnon 2007). As temperatures continue to rise, the
643 atmospheric moisture-holding capacity will increase, favoring more intense precipitation events,
644 potentially even snowstorms (CMAP 2013). The current study provides support for an
645 intensification of snowstorms during this century. Heavy daily snow events are projected to

646 increase in frequency, particularly across the Plains and Prairie Potholes LCC and the Upper
647 Midwest and Great Lakes LCC and most notably for low-warming scenarios.

648 Several limitations are identified in the study. SNOW-17 only requires inputs of ground-
649 level temperature and precipitation, yet it is recognized that ground-level temperature is not a
650 perfect indicator of the form of precipitation (Anderson 2006). SNOW-17 requires an extensive
651 set of spatially-explicit parameters, which can be challenging to develop as most prior model
652 applications focused on single watersheds. The applied parameter values result in insufficient
653 snowmelt and excessive snow depth in spring. The LCC statistical downscaling is based on
654 output from a small set of nine CMIP3 GCMs, rather than the latest CMIP5 archive. Only one
655 realization for each CMIP3 model is considered; thus, the full range of possible climate
656 outcomes may be insufficiently represented. This is particularly a concern for projections out to
657 the mid-21st century, given the importance of internal natural variability on the decadal to multi-
658 decadal time scale (Deser et al. 2012a,b, 2013); future studies should consider large ensemble
659 sets to represent uncertainty. Furthermore, the snowfall projections presented here need to be
660 considered with caution for the Great Lakes Basin, given that the statistical downscaling does not
661 consider future changes in lake ice cover and turbulent fluxes, which regulate lake-effect snow.
662 Observations have shown a positive trend in lake-effect snowfall in the basin (Norton and
663 Bolsenga 1993; Leathers and Ellis 1996; Burnett et al. 2003), in response to greater lake
664 evaporation, although an observed trend reversal towards less lake-effect snowfall might have
665 recently begun (Bard and Kristovich 2012). To address future changes in lake-effect snow, a
666 combination of dynamical downscaling, using regional climate models coupled to interactive
667 lakes (Notaro et al. 2013), and improved statistical downscaling techniques are encouraged.

668
669 Acknowledgements

670 The research was funded by the Upper Midwest and Great Lakes Landscape
671 Conservation Cooperative, Wisconsin Focus on Energy, and the U.S. Environmental Protection
672 Agency's Great Lakes Restoration Initiative through a contract with the Michigan Department of
673 Natural Resources. CMIP3 data was obtained through the Program for Climate Model Diagnosis
674 and Intercomparison (PCMDI). The authors appreciate the helpful comments from three
675 anonymous reviewers. Nelson Institute Center for Climatic Research contribution #.

676

677 References

- 678 Abraham, K. F., R. L. Jefferies, and R. T. Alisauskas, 2005: The dynamics of landscape change
679 and snow geese in mid-continent North America. *Global Change Biology*, 11, 841-855.
- 680 Adeloye, A. J., N. R. Nawaz, and M. Montaseri, 1999: Climate change water resources planning
681 impacts incorporating reservoir surface net evaporation fluxes: A case study. *Water Resourc.*
682 *Dev.*, 15, 561-581.
- 683 Anderson, E. A., 1973: National Weather Service River Forecast System-Snow Accumulation
684 and Ablation Model. NOAA Technical Memorandum: NWS Hydro-17, US National Weather
685 Service.
- 686 Anderson, E. A., 1976: A point energy and mass balance model of a snow cover. NOAA
687 Technical Report NWS 19, 150 pp., February 1976.
- 688 Anderson, E. A., 2002: Calibration of conceptual hydrologic models for use in river forecasting.
689 Office of Hydrologic Development, US National Weather Service, Silver Spring, MD.
- 690 Anderson, E. A., 2006: Snow Accumulation and Ablation Model – SNOW 17. US National
691 Weather Service, Silver Spring, MD.
- 692 Auer, A. H., 1974: The rain versus snow threshold temperatures. *Weatherwise*, 27, 67.

- 693 Bard, L., and D. A. Kristovich, 2012: Trend reversal in Lake Michigan contribution to snowfall.
- 694 *Journal of Applied Meteorology and Climatology*, 51, 2038-2046.
- 695 Barnett, T. P., J. C. Adam, and D. P. Lettenmaier, 2006: Potential impacts of a warming climate
- 696 on water availability in snow-dominated regions. *Nature*, 438, 1-7.
- 697 Baxter, M. A., C. E. Graves, and J. T. Moore, 2005: A climatology of snow-to-liquid ratio for the
- 698 contiguous United States. *Wea. Forecasting*, 20, 729-744.
- 699 Brekke, L. D., E. P. Maurer, J. D. Anderson, M. D. Dettinger, E. S. Townsley, A. Harrison, and
- 700 T. Pruitt, 2009: Assessing reservoir operations risk under climate change. *Water Resources*
- 701 *Research*, 45, W04411, doi:10.1029/2008WR006941.
- 702 Brown, R. D., 2000: Northern Hemisphere snow cover variability and change, 1915-97. *J. Clim.*,
- 703 13, 2339-2355.
- 704 Brown, R. D., and P. W. Mote, 2009: The response of Northern Hemisphere snow cover to a
- 705 changing climate. *J. Clim.*, 22, 2124-2145.
- 706 Brutel-Vuilmet, C., M. Ménégoz, and G. Krinner, 2013: An analysis of present and future
- 707 seasonal Northern Hemisphere land snow cover simulated by CMIP5 coupled climate models.
- 708 *The Cryosphere*, 7, 67-80.
- 709 Burnash, R. J. C., R. L. Ferral, and R. A. McQuire, 1973: A generalized streamflow simulation
- 710 system – conceptual modeling for digital computers. Joint Federal and State River Forecast
- 711 Center, U.S. National Weather Service and California Department of Water Resources,
- 712 Sacramento, California, p. 204.
- 713 Burnett, A. W., M. E. Kirby, H. T. Mullins, and W. P. Patterson, 2003: Increasing Great Lake-
- 714 effect snowfall during the twentieth century: A regional response to global warming? *J. Clim.*,
- 715 16, 3535-3542.

- 716 Carroll, C., 2007: Interacting effects of climate change, landscape conversion, and harvest on
717 carnivore populations at the range margin: Marten and lynx in the northern Appalachians.
718 *Conservation Biology*, 21, 1092-1104.
- 719 Changnon, S. A., 1969: Climatology of severe winter storms in Illinois. Illinois State Water
720 Survey, Bulletin 53, State of Illinois, Department of Registration and Education, Urbana,
721 Illinois, 45 pp.
- 722 Changnon, S. A., 2007: Catastrophic winter storms: An escalating problem. *Climatic Change*,
723 84, 131-139.
- 724 Changnon, S. A., D. Changnon, and T. R. Karl, 2006: Temporal and spatial characteristics of
725 snowstorms in the contiguous U.S. *J. Appl. Meteorol. Clim.*, 45, 1141–1156.
- 726 Christensen, J.H., et al., 2007: Regional climate projections. In: Climate Change 2007: The
727 Physical Science Basis. Contribution of Working Group 1 to the Fourth Assessment Report of
728 the Intergovernmental Panel on Climate Change [Solomon S, Qin D, Manning M, Chen Z,
729 Marquis M, Averyt KB, Tignor M, Miller HL (eds.)]. Cambridge University Press,
730 Cambridge, United Kingdom and New York, NY, USA.
- 731 CMAP, 2013: Climate adaptation guidebook for municipalities in the Chicago region. June 2013.
- 732 Cox, H. J., and J. H. Armington, 1914: The weather and climate of Chicago. Chicago, University
733 of Chicago Press, 375 pp.
- 734 Daly, C., 2006: Guidelines for assessing the suitability of spatial climate data sets. *Int. J.*
735 *Climatol.*, 26, 707-721.
- 736 Daly C., W. P. Gibson, G. H. Taylor, M. K.. Doggett, and J. I. Smith, 2007: Observer bias in
737 daily precipitation measurements at United States cooperative network stations. *Bulletin of the*
738 *American Meteorological Society*, 88, 899–912.

- 739 Daly, C., et al., 2008: Physiographically sensitive mapping of climatological temperature and
740 precipitation across the conterminous United States. *International Journal of Climatology*, 28,
741 2031-2064.
- 742 Delworth, T. L., and Coauthors, 2006: GFDL's CM2 global coupled climate models. Part I:
743 Formulation and simulation characteristics. *J. Clim.*, 19, 643–674.
- 744 Déqué, M., C. Dreveton, A. Braun, and D. Cariolle, 1994: The ARPEGE–IFS atmosphere model:
745 A contribution to the French community climate modelling. *Climate Dyn.*, 10, 249–266.
- 746 Deser, C., R. Knutti, S. Solomon, and A. S. Phillips, 2012a: Communication of the role of
747 natural variability in future North American climate. *Nature Climate Change*,
748 doi:10.1038/NCLIMATE1562.
- 749 Deser, C., A. Phillips, V. Bourdette, and H. Teng, 2012b: Uncertainty in climate change
750 projections: the role of internal variability. *Climate Dynamics*, 38, 527-546.
- 751 Deser, C., A. S. Phillips, M. A. Alexander, and B. V. Smoliak, 2013: Projecting North American
752 climate over the next 50 years: Uncertainty due to internal variability. *J. Clim.*, in review.
- 753 Draper, S. E., and J. E. Kundell, 2007: Impact of climate change on transboundary water sharing.
754 *J. Water Resour. Plann. Manage.*, 133, 405-415.
- 755 Edwards, R. Y., 1956: Snow depths and ungulate abundance in the mountains of western Canada.
756 *J. Wildl. Mgmt.*, 20, 159-168.
- 757 Eisenberg, D., and K. E. Warner, 2005: Effects of snowfalls on motor vehicle collisions, injuries,
758 and fatalities. *Amer. J. Public Health*, 95, 120-124.
- 759 Flato, G. M., G. J. Boer, W. G. Lee, N. A. McFarlane, D. Ramsden, M. C. Reader, and A. J.
760 Weaver, 2000: The Canadian Centre for Climate Modeling and Analysis global coupled model
761 and its climate. *Climate Dyn.*, 16, 451–467.

- 762 Franz, K. J., T. S. Hogue, and S. Sorooshian, 2008a: Snow model verification using ensemble
763 prediction and operational benchmarks. *Journal of Hydrometeorology*, 9, 1402-1415.
- 764 Franz, K. J., T. S. Hogue, and S. Sorooshian, 2008b: Operational snow modeling: Addressing the
765 challenges of an energy balance model for National Weather Service forecasts. *Journal of
766 Hydrology*, 360, 48-66.
- 767 Gordon, H.B., and S.P. O'Farrell, 1997: Transient climate change in the CSIRO coupled model
768 with dynamic sea ice. *Mon. Wea. Rev.*, 125, 875-907.
- 769 Gordon, H. B., and Coauthors, 2002: The CSIRO Mk3 Climate System Model. CSIRO
770 Atmospheric Research Tech. Rep. 60, 130 pp.
- 771 Grado, S. C., K. M. Hunt, C. P. Hutt, X. T. Santos, and R. M. Kaminiski, 2011: Economic
772 impacts of waterfowl hunting in Mississippi derived from a state-based mail survey. *Human
773 Dimensions of Wildlife*, 16, 100-113.
- 774 Groisman, P. Ya, R. W. Knight, T. R. Karl, and R. R. Heim Jr, 1993: Inferences of the North
775 American snowfall and snow cover with recent global temperature changes. Proc. Snow
776 Watch '92 Int. Workshop, Niagara-on-the-Lake, Canada, Canadian Climate Centre, WMO,
777 and Institute for Space and Terrestrial Science, 44-51.
- 778 Groisman, P. Y., R. W. Knight, and T. R. Karl, 2001: Heavy precipitation and high streamflow
779 in the contiguous United States: Trends in the twentieth century. *Bull. Amer. Meteor. Soc.*,
780 82, 219-246.
- 781 Gutowski, W. J., et al., 2008: Causes of Observed Changes in Extremes and Projections of
782 Future Changes in Weather and Climate Extremes in a Changing Climate. Regions of Focus:
783 North America, Hawaii, Caribbean, and U.S. Pacific Islands. T.R. Karl, G.A. Meehl, C.D.
784 Miller, S.J. Hassol, A.M. Waple, and W.L. Murray (eds.). A Report by the U.S. Climate

- 785 Change Science Program and the Subcommittee on Global Change Research, Washington, DC.
- 786 Hanson, R. T., L. E. Flint, A. L. Flint, M. D. Dettinger, C. C. Faunt, D. Cayan, and W. Schmid,
- 787 2012: A method for physically based model analysis of conjunctive use in response to
- 788 potential climate changes. *Water Resources Research*, 48, W00L08,
- 789 doi:10.1029/2011WR010774.
- 790 He, M., T. S. Hogue, K. J. Franz, S. A. Margulis, and J. A. Vrugt, 2011: Characterizing
- 791 parameter sensitivity and uncertainty for a snow model across hydroclimatic regimes.
- 792 *Advances in Water Resources*, 34, 114-127.
- 793 Hoving, C. L., D. J. Harrison, W. B. Krohn, R. A. Joseph, and M. O'Brien, 2005: Broad-scale
- 794 predictors of Canada lynx occurrence in eastern North America. *Journal of Wildlife*
- 795 *Management*, 69, 739-751.
- 796 Kalnay, E., et al., 1996: The NCEP/NCAR 40-year reanalysis project. *Bulletin of the American*
- 797 *Meteorological Society*, 77, 437-471.
- 798 Kapnick, S., and T. Delworth, 2013: Controls of global snow under a changed climate. *J. Clim.*,
- 799 doi:10.1175/JCLI-D-12-00528.1, in press.
- 800 Kitoh, A., A. Noda, Y. Nikaidou, T. Ose, and T. Tokioka, 1995: AMIP simulations of the MRI
- 801 GCM. *Pap. Meteor. Geophys.* 45, 121–148.
- 802 Knapp, K. K., D. Kroeger, and K. Giese, 2000: Mobility and safety impacts of winter storm
- 803 events in a freeway environment: Final report. Center for Transportation Research and
- 804 Education, Iowa State University, 76 pp.
- 805 Kohn, B., 1975: Winter severity measurements. Wisconsin Department of Natural Resources
- 806 Final Report Job 210.4, P-R Proj. W-141-R-10, 11 pp.
- 807 Krasting, J., A. Broccoli, K. Dixon, and J. Lanzante, 2013: Future changes in Northern

- 808 Hemisphere snowfall. *J. Clim.*, doi:10.1175/JCLI-D-12-00832.1, in press.
- 809 Krohn, W. B., C. L. Hoving, D. J. Harrison, D. M. Phillips, and H. C. Frost, 2004: Martes foot-
810 loading and snowfall patterns in eastern North America: Implications to broad-scale
811 distributions and interactions of mesocarnivores. In D.J. Harrison and A.K. Fuller, editors.
812 Martes in human altered landscapes – Proceedings of the Third International Martes
813 Symposium, Columbia University Press, New York.
- 814 Kunkel, K. E., N. E. Wescott, and D. A. R. Kristovich, 2000: Climate change and lake-effect
815 snow. Preparing for a Changing Climate: The Potential Consequences of Climate Variability
816 and Change, P. J. Sousounis, and J. M. Bisanz, Eds., U.S. EPA, Office of Research and
817 Development Global Change Research Program, 25–28.
- 818 Kutikoff, S. L., 2013: A climatology of lake-effect snowfall and evaluation of the Cobb method
819 for the Great Lakes region. Thesis, University of Nebraska, 62 pp.
- 820 Laird, N., R. Sobash, and N. Hodas, 2009: The frequency and characteristics of lake-effect
821 precipitation events associated with the New York State Finger Lakes. *Journal of Applied
822 Meteorology and Climatology*, 48, 873-886.
- 823 Leathers, D. J., and A. W. Ellis, 1996: Synoptic mechanisms associated with snowfall increases
824 to the lee of Lakes Erie and Ontario. *Int. J. Climate*, 16, 1117-1135.
- 825 Legutke, S., and R. Voss, 1999: The Hamburg atmosphere-ocean coupled circulation model
826 ECHO-G. Technical Report, No. 18, German Climate Computer Centre (DKRZ), Hamburg,
827 62 pp.
- 828 Lemke, P., et al., 2007: Observations: Changes in snow, ice and frozen ground. In: Climate
829 Change 2007: The Physical Science Basis. Contribution of Working Group 1 to the Fourth
830 Assessment Report of the Intergovernmental Panel on Climate Change [Solomon S, Qin D,

- 831 Manning M, Chen Z, Marquis M, Averyt KB, Tignor M, Miller HL (eds.)]. Cambridge
832 University Press, Cambridge, United Kingdom and New York, NY, USA.
- 833 Lettenmaier, D., and T. Gan, 1990: Hydrologic sensitivities of the Sacramento-San Joaquin
834 River basin, California, to global warming. *Water Resourc. Res.*, 26, 69-86.
- 835 Link, W. A., J. R. Sauer, and D. K. Niven, 2006: A hierarchical model for regional analyses of
836 population change using Christmas Bird Count data, with application to the American black
837 duck. *Condor*, 108, 13-24.
- 838 López-Moreno, J. I., S. Goyette, S. M. Vicente-Serrano, and M. Beniston, 2011: Effects of
839 climate change on the intensity and frequency of heavy snowfall events in the Pyrenees.
840 *Climatic Change*, 105, 489-508.
- 841 Mahanama, S., B. Livneh, R. Koster, D. Lettenmaier, and R. Reichle, 2011: Soil moisture, snow,
842 and seasonal streamflow forecasts in the United States. *Journal of Hydrometeorology*, 13,
843 189-203.
- 844 Manabe, S., R. T. Wetherald, and R. J. Stouffer, 1981: Summer dryness due to an increase of
845 atmospheric CO₂ concentration. *Climatic Change*, 3, 347-386.
- 846 Mastin, M. C., K. J. Chase, and R. W. Dudley, 2011: Changes in spring snowpack for selected
847 basins in the United States for different climate-change scenarios. *Earth Interactions*, 15, 1-18.
- 848 Maurer, E. P., L. D. Brekke, and T. Pruitt, 2010: Contrasting lumped and distributed hydrology
849 models for estimating climate change impacts on California watersheds. *Journal of the
850 American Water Resources Association*, 46, 1024-1035.
- 851 Maurer, E. P., I. T. Stewart, C. Bonfils, P. B. Duffy, and D. Cayan, 2007: Detection, attribution,
852 and sensitivity of trends toward earlier streamflow in the Sierra Nevada. *J. Geophysical
853 Research*, 112, D11118, doi:10.1029/2006JD008088.

- 854 McKenney, D. W., M. F. Hutchinson, J. L. Kesteven, and L. A. Venier, 2001: Canada's plant
855 hardiness zones revisited using modern climate interpolation techniques. *Canadian Journal of*
856 *Plant Science*, 81, 129-143.
- 857 Mesinger, F., et al., 2006: North American Regional Reanalysis. *Bull. Amer. Meteor. Soc.*, 87,
858 343-360.
- 859 Miller, N. L., K. E. Bashford, and E. Strem, 2003: Potential impacts of climate change on
860 California hydrology. *Journal of the American Water Resources Association*, August 2003,
861 771-784.
- 862 Mishra, V., K. A. Cherkauer, and S. Shukla, 2010: Assessment of drought due to historic climate
863 variability and projected future climate change in the midwestern United States. *Journal of*
864 *Hydrometeorology*, 11, 46-68.
- 865 Mitchell, K. E., et al., 2005: Community Noah Land Surface Model (LSM) – User's guide
866 (v2.7.1). [Available online at ftp://ftp.emc.ncep.noaa.gov/mmb/gcp/ladas/noahlsm/ver_2.7.1].
- 867 National Geophysical Data Center, 2013: 2-minute gridded global relief data (ETOPO2v2).
868 NOAA/NESDIS/NGCD. [Available online at
869 <http://www.ngdc.noaa.gov/mgg/fliers/06mgg01.html>].
- 870 Norton, D. C., and S. J. Bolsenga, 1993: Spatiotemporal trends in lake effect and continental
871 snowfall in the Laurentian Great Lakes, 1951-1980. *J. Climate*, 6, 1943-1955.
- 872 Notaro, M., D. Lorenz, D. Vimont, S. Vavrus, C. Kucharik, and K. Franz, 2011: 21st century
873 Wisconsin snow projections based on an operational snow model driven by statistically
874 downscaled climate data. *J. Climatol.*, 31, 1615-1633.
- 875 Notaro, M., A. Zarrin, S. Vavrus, and V. Bennington, 2013: Simulation of heavy lake-effect
876 snowstorms across the Great Lakes Basin by RegCM4: Synoptic climatology and variability.

- 877 *Monthly Weather Review*, 141, 1990-2014.
- 878 NWS (National Weather Service) National Weather Service River Forecast System User Manual,
879 2005.
- 880 O'Gorman, P. A., and T. Schneider, 2009: The physical basis for increases in
881 precipitation extremes in simulations of 21st-century climate change. *Proceedings of*
882 *the National Academy of Sciences*, 106, 14773-14777.
- 883 Ohmura, A., 2001: Physical basis for the temperature-based melt index method. *J. Appl.*
884 *Meteorol.*, 40, 753-761.
- 885 Peacock, S., 2012: Projected twenty-first-century changes in temperature, precipitation, and
886 snow cover over North America in CCSM4. *J. Clim.*, 25, 4405-4429.
- 887 Raleigh, M. S., and J. D. Lundquist, 2012: Comparing and combining SWE estimates from the
888 SNOW-17 model using PRISM and SWE reconstruction. *Water Resour. Res.*, 48, W01506.
- 889 Rasmussen, R. M., A. Crook, and C. Kessinger, 1993: Snow-band formation and evolution during
890 the 15 November 1987 aircraft accident at Denver airport. *Weather and Forecasting*, 8, 453-
891 480.
- 892 Robinson, P. J., 1989: The influence of weather on flight operations at the Atlanta Hartsfield
893 International Airport. *Weather and Forecasting*, 4, 461-468.
- 894 Räisänen, J., 2007: Warmer climate: Less or more snow? *Climate Dynamics*, 30, 307-319,
895 doi:10.1007/s00382-007-02890-y.
- 896 Raleigh, M. S., and J. D. Lundquist, 2012: Comparing and combining SWE estimates from the
897 SNOW-17 model using PRISM and SWE reconstruction. *Water Resources Research*, 48,
898 W01506, doi:10.1029/2011WR010542.
- 899 Roeckner, E., et al., 2003: The atmospheric general circulation model ECHAM5. Part I: Model

- 900 description. Max Planck Institute for Meteorology Rep., 349, 127 pp. [available from MPI for
901 Meteorology, Bundesstr, 53, 20146, Hamburg, Germany].
- 902 Roesch, A., 2006: Evaluation of surface albedo and snow cover in AR4 coupled climate models.
903 *J. Geophys. Res.*, 111, D15111, doi:10.1029/2005JD006473.
- 904 Rogot, E., and S. J. Padgett, 1976: Associations of coronary and stroke mortality with
905 temperature and snowfall in selected areas of the United States, 1962-1966. *Amer. J.*
906 *Epidemiology*, 103, 565-575.
- 907 Rooney, J. F., 1967: Urban snow hazard in the United States – appraisal of disruption.
908 *Geographical Rev.*, 57, 538-559.
- 909 Schmidt, G. A., et al., 2005: Present day simulations using GISS ModelE: Comparison to in-situ,
910 satellite and reanalysis data. *J. Clim.*, 19, 153-192.
- 911 Schummer, M. L., R. M. Kaminski, A. H. Raedeke, and D. A. Gruber, 2010: Weather-related
912 indices of autumn-winter dabbling duck abundance in middle North America. *Journal of*
913 *Wildlife Management*, 74, 94-101.
- 914 Scott, D., J. Dawson, and B. Jones, 2008: Climate change vulnerability of the US Northeast
915 winter recreation-tourism sector. *Mitigation and Adaptation Strategies for Global Change*,
916 13, 577-596.
- 917 Severinghaus, C. W., 1947: Relationship of weather to winter mortality and population levels
918 among deer in the Adirondack region of New York. *Trans. N. Am. Wildl. Conf.*, 12, 212-223.
- 919 Snow Hydrology, 1956: Summary Report of the Snow investigations, North Pacific Division,
920 Corps of Engineers, Portland, Oregon, 437 pp., June 1956.
- 921 Southwick Associates, 2012: Hunting in America: An economic force for conservation.
922 Produced for National Shooting Sports Foundation in partnership with the Association of Fish

- 923 and Wildlife Agencies.
- 924 Stacy, E. W., 1962: A generalization of the gamma distribution. *The Annals of Mathematical*
925 *Statistics*, 33, 1187–1192.
- 926 Švažas, S., R. Patapavičius, and M. Dagys, 2001: Recent changes in distribution of wintering
927 populations of waterfowl established on the basis of Lithuanian ringing recoveries. *Acta*
928 *Zoologica Lituanica*, 11, 235-242.
- 929 U.S. Department of the Interior, U.S. Fish and Wildlife Service, and U.S. Department of
930 Commerce, U.S. Census Bureau, 2011: National Survey of Fishing, Hunting, and Wildlife-
931 Associated Recreation.
- 932 Verme, L. J., 1968: An index of winter weather severity for northern deer. *J. Wildl. Manage.*,
933 32, 566-574.
- 934 Vicuna, S., R. Leonardson, M. Hanemann, L. Dale, and J. Dracup, 2008: Climate change impacts
935 on high elevation hydropower generation in California's Sierra Nevada: A case study on the
936 Upper American River. *Climatic Change*, 87, 123-137.
- 937 Westerling, A., H. Hidalgo, D. Cayan, and T. Swetnam, 2006: Warming and earlier spring
938 increases western US forest wildfire activity. *Science*, 313, 940-943.
- 939 Wisconsin's Changing Climate: Impacts and Adaptation (WICCI), 2011: Wisconsin Initiative on
940 Climate Change Impacts. Nelson Institute for Environmental Studies, University of
941 Wisconsin-Madison and the Wisconsin Department of Natural Resources, Madison,
942 Wisconsin.
- 943 Wood, A.W., E. P. Maurer, A. Kumar, and D. P. Lettenmaier, 2002: Long range experimental
944 hydrologic forecasting for the eastern U.S., *J. Geophysical Research*, 107, D20, 4429.
- 945 Wood, A. W., L. R. Leung, V. Srifhar, and D. P. Lettenmaier, 2004: Hydrologic implications od

946 dynamical and statistical approaches to downscaling climate model outputs. *Climatic Change*,
947 62, 189-216.
948 Zappa, M., F. Pos, U. Strasser, P. Warmerdam, and J. Gurtz, 2003: Seasonal water balance of an
949 Alpine catchment as evaluated by different methods for spatially distributed snowmelt
950 modeling. *Nord. Hydrol.*, 34, 179-202.
951 Zhang, Y., S. Wang, A. G. Barr, and T. A. Black, 2008: Impact of snow cover on soil
952 temperature and its simulation in a boreal aspen forest. *Cold Reg. Sci. Technol.*, 52, 355-370.

953

954

955

956

957

958

959

960

961 Figure Captions

962

963 Fig. 1 Map of elevation (m), based on ETOP02 global topographic grid, with red polygons
964 outlining the relevant LCCs and black dots for 196 stations. Snowfall climatology at these
965 stations is used to assess the performance of SNOW-17 and estimate the SCF parameter. The 10
966 LCC regions of interest are identified by number. For each LCC region, the largest populated
967 city is identified.

968

969 Fig. 2 Scatter plots of observed versus simulated (a) annual snowfall (cm) and (b) DJF snow
970 depth for 196 stations, based on a climatology for 1981-2000. For snowfall (snow depth), the
971 temporal correlation is 0.99 (0.90) and root-mean-square-difference is 5.9 cm (4.4 cm). Scatter
972 plots for individual months are shown for (a1-6) snowfall and (b1-6) snow depth, with the
973 correlation coefficient provided in each panel.

974

975 Fig. 3 Projected change in DJFM mean temperature ($^{\circ}$ C) by the late 21st century, computed as
976 the difference between 2081-2100 and 1981-2000. Results are shown for the (a-d) A2 and (e-h)
977 B1 emission scenarios and are broken down by (a,e) low-end projection, (b,f) mean projection,
978 (c,g) high-end projection, and (d,h) spread (difference between high-end and low-end
979 projections) per grid cell. Among nine GCMs, the greatest warming at each grid cell is
980 considered high-end and the least warming is considered low-end. The upper color bar pertains
981 to (a-c, e-g) and the lower color bar pertains to (d,h). All of the differences shown in (a-c, e-g)
982 are statistically significant ($p < 0.1$), except over central Montana and southern Alberta in (e).

983

984 Fig. 4 Projected change in DJFM mean precipitation (mm/day) by the late 21st century,
985 computed as the difference between 2081-2100 and 1981-2000. Results are shown for the (a-d)
986 A2 and (e-h) B1 emission scenarios and are broken down by (a,e) low-end projection, (b,f) mean
987 projection, (c,g) high-end projection, and (d,h) spread (difference between high-end and low-end
988 projections) per grid cell. Among nine GCMs, the greatest increase in precipitation at each grid
989 cell is considered high-end and the greatest drying (or least increase in precipitation) is
990 considered low-end. The upper color bar pertains to (a-c, e-g) and the lower color bar pertains to
991 (d,h). Statistically significant differences in (a-c, e-g) are dotted ($p < 0.1$).

992

993 Fig. 5 Simulated daily precipitation (mm) and 850-hPa wind vectors from a select day in (a)
994 December 1989 from the 20C3M simulation of GISS Model E-R and a select day in (b)
995 December 1987 from the 20C3M simulation of MPI ECHAM5, which include northwesterly
996 winds over the Great Lakes which should support lake-effect snowfall. Reference vectors are
997 assigned values of (a) 5 m/s and (b) 10 m/s. For these two events, simulated snowfall (cm) is
998 shown in (c) for the GISS model and (d) for the MPI model, based on SNOW-17 simulations
999 forced by downscaled climate data. Lake-effect precipitation is absent in (a-b) but captured in
1000 (c-d).

1001

1002 Fig. 6 Climatological mean annual snowfall (cm) from the (a) raw CMIP3 GCMs, (b)
1003 downscaled SNOW-17, and (c) 196 weather stations for 1981-2000. Since the GCMs only saved
1004 liquid-equivalent of snowfall, a 10:1 ratio was applied to crudely estimate simulated snowfall.

1005

1006 Fig. 7 Projected change in annual snowfall (cm) by the (a-c,g-i) mid-21st century (2046-2065)
1007 and (d-f,j-l) late 21st century (2081-2100), computed as the difference from the late 20th century
1008 (1981-2000), according to the (a-f) B1 and (g-l) A2 emission scenarios. Results are broken
1009 down by (a,d,g,j) low-end, (b,e,h,k) mean, and (c,f,i,l) high-end projections per grid cell. Among
1010 the nine GCMs, the largest decline in snowfall at each grid cell is considered high-end and the
1011 greatest increase (or smallest decline) is considered low-end.

1012

1013 Fig. 8 Mean projected percentage change in the annual (a-d) frequency of daily snowfall events
1014 of at least 1 cm and (e-h) mean snowfall per event by the (a,e,c,g) mid-21st century (2046-2065)

1015 and (b,f,d,h) late 21st century (2081-2100), compare to the late 20th century (1981-2000).
1016 Results are shown both for the (a-b,e-f) B1 and (c-d,g-h) A2 emission scenarios. The median
1017 projections are also computed (not shown) and found to be quite consistent with the mean
1018 projections shown here.

1019

1020 Fig. 9 Projected percentage change in the frequency of daily snowfall (cm) events, within the
1021 entire 10 LCC study region (blue lines) and the region encompassing the Plains and Prairie
1022 Potholes LCC and Upper Midwest and Great Lakes LCC (red lines). Projections are shown for
1023 the (a-b) B1 and (c-d) A2 scenarios and for the (a,c) mid-21st and (b,d) late 21st century. The x-
1024 axis consists of 1-cm daily snowfall bins (0.1-1, 1-2, 2-3,..., 99-100) for the former region and 2-
1025 cm bins (0.1-2, 2-4, 4-6,..., 98-100) for the latter region. Thin black curves are also included for
1026 each of the following LCC regions: Appalachian, Eastern Tallgrass Prairie and Big Rivers,
1027 Plains and Prairie Potholes, Great Plains, Upper Midwest and Great Lakes, and North Atlantic.

1028

1029 Fig. 10 Month of maximum projected decline in snowfall, according to the A2 emission
1030 scenario by the end of the 21st century (2081-2100), compared to the late 20th century (1981-
1031 2000). SNOW-17 is forced by downscaled climate projections from nine GCMs, the mean
1032 snowfall projection is computed among these models, and then the month of maximum decline
1033 in snowfall is identified.

1034

1035 Fig. 11 Projected percentage change in NDJFMA mean snow depth by the (a-c,g-i) mid-21st
1036 century (2046-2065) and (d-f,j-l) late 21st century (2081-2100), computed as the difference from
1037 the late 20th century (1981-2000), according to the (a-f) B1 and (g-l) A2 emission scenarios.

1038 Results are broken down by (a,d,g,j) low-end, (b,e,h,k) mean, and (c,f,i,l) high-end projections
1039 per grid cell. Among the nine GCMs, the largest decline in snow depth at each grid cell is
1040 considered high-end and the greatest increase (or smallest decline) is considered low-end.

1041

1042 Fig. 12 Mean projected change in the number of days per year with a minimum snowpack of 1
1043 cm by the (a,c) mid-21st century (2046-2065) and (b,d) late 21st century (2081-2100), compared
1044 to the late 20th century (1981-2000). Results are shown for the (a-b) B1 and (c-d) A2 emission
1045 scenarios. The green curve represents the -5°C mean isotherm for DJFM for 1981-2000. Scatter
1046 plots display (y-axis) mean climatological DJFM temperature (°C) from 1981-2000 versus (x-
1047 axis) projected change in number of days per year with a minimum snowpack, with a dot for
1048 each grid cell.

1049

1050 Fig. 13 Ratio of the mean projected change in annual snowfall by the late 21st century (2081-
1051 2100) to the mean projected change by the mid-21st century (2046-2065), compared to the 20th
1052 century (1981-2000). Results are based on the A2 emission scenario. Ratios greater than one
1053 indicate accelerated snowfall declines later in the 21st century. The black dashed line represents
1054 the -5°C mean isotherm for DJFM for 1981-2000.

1055

1056 Fig. 14 (a-f) Mean probability of the daily CWSI in specific LCC regions exceeding 7.2 from
1057 November to March, for the late 20th century (black), mid-21st century (B1 scenario - blue, A2
1058 scenario - green), and late 21st century (B1 - orange, A2 - red), based on mean projections from
1059 nine GCMs. (g-l) Mean CWSI for October-March for the late 20th century. The thick black

1060 lines indicate CWSI=7.2, a critical threshold for mallard ducks. Note that the CWSI is
1061 cumulatively summed each day from 1 September to 31 March.

1062

1063 **Table Captions**

1064

1065 Table 1. Summary of results for five LCC regions: South Atlantic, Peninsular Florida,
1066 Appalachian, Gulf Coastal Plains and Ozarks, and Eastern Tallgrass Prairie and Big Rivers.

1067 Variables include DJFM air temperature (°C), DJFM precipitation (mm/day), annual snowfall
1068 (cm), NDJFMA mean snow depth (cm), number of days per year with snowfall of at least 1 cm,
1069 average snowfall per event (cm), number of days per year with a snowpack of at least 1 cm, and
1070 cumulative WSI. Results are based on the statistical downscaling data and SNOW-17
1071 simulations. For the first seven variables, Mod represents the late 20th century mean value and
1072 A2 and B1 represent projected changes (both actual change and percentage change) by the end of
1073 the century (2081-2100 versus 1981-2000). For cumulative WSI, Mod represents the mean WSI
1074 value for 1981-2000, while A2 and B1 represent the mean WSI value for 2081-2100 for two
1075 emission scenarios.

1076

1077 Table 2. Same as table 1, except for five other LCC regions: Plains and Prairie Potholes, Great
1078 Plains, Gulf Coast Prairie, Upper Midwest and Great Lakes, and North Atlantic.

1079

1080 Table 3. List of the nine global climate models analyzed in this study.

Tables 1-2

[Click here to download Manuscript \(non-LaTeX\): tables1+2.pdf](#)

	South Atlantic		Peninsular Florida		Appalachian		Gulf Coastal Plains and Ozarks		Eastern Tallgrass Prairie and Big Rivers	
DJFM temperature	Mod	9.16°C	Mod	17.81°C	Mod	2.39°C	Mod	8.36°C	Mod	-0.65°C
	A2	+4.08°C	A2	+5.43°C	A2	+4.67°C	A2	+4.56°C	A2	+5.39°C
	B1	+2.26°C	B1	+2.90°C	B1	+2.72°C	B1	+2.58°C	B1	+3.21°C
DJFM precipitation	Mod	3.32 mm/d	Mod	2.13 mm/d	Mod	3.24 mm/d	Mod	3.70 mm/d	Mod	1.59 mm/d
	A2	+.23 mm/d +7.0%	A2	-.01 mm/d -0.3%	A2	+.46 mm/d +14.3%	A2	+.06 mm/d +1.5%	A2	+.26 mm/d +16.6%
	B1	+.11 mm/d +3.3%	B1	+.16 mm/d +7.8%	B1	+.24 mm/d +7.4%	B1	+.09 mm/d +2.3%	B1	+.18 mm/d +11.2%
Annual snowfall	Mod	10.2 cm	Mod	0.0 cm	Mod	87.1 cm	Mod	15.9 cm	Mod	74.0 cm
	A2	-7.9 cm -77.0%	A2	-0.0 cm -97.8%	A2	-50.7 cm -58.2%	A2	-11.1 cm -69.7%	A2	-40.0 cm -54.1%
	B1	-5.4 cm -52.7%	B1	-0.0 cm -76.8%	B1	-34.1 cm -39.1%	B1	-7.4 cm -46.7%	B1	-27.2 cm -36.8%
NDJFMA snow depth	Mod	0.07 cm	Mod	0.00 cm	Mod	1.99 cm	Mod	0.19 cm	Mod	2.43 cm
	A2	-.06 cm -79.7%	A2	-.00 cm -98.9%	A2	-1.53 cm -76.6%	A2	-.14 cm -74.8%	A2	-1.69 cm -69.4%
	B1	-.04 cm -56.1%	B1	-.00 cm -82.3%	B1	-1.18 cm -59.0%	B1	-.10 cm -54.9%	B1	-1.28 cm -52.6%
# snow days per year	Mod	1.91 dys	Mod	0.01 dys	Mod	15.26 dys	Mod	3.06 dys	Mod	13.61 dys
	A2	-1.47 dys -77.0%	A2	-0.01 dys -99.1%	A2	-8.72 dys -57.2%	A2	-2.11 dys -69.1%	A2	-7.28 dys -53.5%
	B1	-1.01 dys -53.1%	B1	-0.01 dys -75.1%	B1	-5.66 dys -37.1%	B1	-1.45 dys -47.4%	B1	-4.80 dys -53.5%
Average snowfall per event	Mod	4.26 cm	Mod	2.39 cm	Mod	4.94 cm	Mod	4.34 cm	Mod	5.04 cm
	A2	-0.49 cm -11.6%	A2	-1.36 cm -57.0%	A2	-0.38 cm -7.6%	A2	-0.62 cm -14.3%	A2	-0.19 cm -3.7%
	B1	-0.33 cm -7.8%	B1	-0.40 cm -16.5%	B1	-0.21 cm -4.2%	B1	+0.10 cm +2.2%	B1	-0.16 cm -3.3%
# days of snowpack per year	Mod	2.58 dys	Mod	0.00 dys	Mod	32.96 dys	Mod	5.32 dys	Mod	49.65 dys
	A2	-2.07 dys -80.5%	A2	-0.00 dys -100.0%	A2	-22.13 dys -67.1%	A2	-3.86 dys -72.7%	A2	-29.81 dys -60.0%
	B1	-1.51 dys -58.6%	B1	-0.00 dys -88.0%	B1	-15.25 dys -46.3%	B1	-2.72 dys -51.1%	B1	-20.24 dys -40.8%
Cumulative WSI	Mod	-8.9	Mod	-17.8	Mod	4.9	Mod	-7.7	Mod	15.0
	A2	-13.2	A2	-23.3	A2	-5.8	A2	-12.8	A2	-1.3
	B1	-11.3	B1	-20.7	B1	-2.4	B1	-10.7	B1	3.5

Table 1. Summary of results for five LCC regions: South Atlantic, Peninsular Florida, Appalachian, Gulf Coastal Plains and Ozarks, and Eastern Tallgrass Prairie and Big Rivers. Variables include DJFM air temperature (°C), DJFM precipitation (mm/day), annual snowfall (cm), NDJFMA mean snow depth (cm), number of days per year with snowfall of at least 1 cm, average snowfall per event (cm), number of days per year with a snowpack of at least 1 cm, and cumulative WSI. For the first seven variables, Mod represents the late 20th century mean value and A2 and B1 represent projected changes (both actual change and percentage change) by the end of the century (2081-2100 versus 1981-2000). For cumulative WSI, Mod represents the mean WSI value for 1981-2000, while A2 and B1 represent the mean WSI value for 2081-2100 for two emission scenarios.

	Plains and Prairie Potholes		Great Plains		Gulf Coast Prairie		Upper Midwest and Great Lakes		North Atlantic	
DJFM temperature	Mod	-7.54°C	Mod	2.57°C	Mod	11.60°C	Mod	-7.70°C	Mod	-3.12°C
	A2	+5.68°C	A2	+5.06°C	A2	+4.69°C	A2	+5.97°C	A2	+5.29°C
	B1	+3.60°C	B1	+2.92°C	B1	+2.53°C	B1	+3.54°C	B1	+3.12°C
DJFM precipitation	Mod	0.44mm/d	Mod	0.65mm/d	Mod	1.82mm/d	Mod	1.53mm/d	Mod	2.79mm/d
	A2	+1.10mm/d +22.4%	A2	+0.00mm/d +0.6%	A2	-.19mm/d -10.7%	A2	+.36mm/d +23.4%	A2	+.61mm/d +21.7%
	B1	+.05mm/d +12.1%	B1	+.02mm/d +3.6%	B1	-.04mm/d -2.0%	B1	+.23mm/d +14.8%	B1	+.34mm/d +12.1%
Annual snowfall	Mod	113.7 cm	Mod	63.6 cm	Mod	7.9 cm	Mod	223.9 cm	Mod	191.2 cm
	A2	-39.1 cm -34.4%	A2	-32.1 cm -50.5%	A2	-5.5 cm -70.2%	A2	-89.9 cm -40.2%	A2	-92.0 cm -48.1%
	B1	-25.8 cm -22.7%	B1	-20.4 cm -32.2%	B1	-3.7 cm -46.5%	B1	-53.9 cm -24.1%	B1	-58.8 cm -30.8%
NDJFMA snow depth	Mod	6.48 cm	Mod	1.06 cm	Mod	0.07 cm	Mod	20.66 cm	Mod	13.63 cm
	A2	-3.17 cm -49.0%	A2	-.67 cm -63.0%	A2	-.05 cm -70.8%	A2	-11.94 cm -57.8%	A2	-9.82 cm -72.1%
	B1	-2.20 cm -34.6%	B1	-.47 cm -44.7%	B1	-.03 cm -52.2%	B1	-7.63 cm -36.9%	B1	-6.89 cm -50.6%
# snow days per year	Mod	21.79 dys	Mod	9.33 dys	Mod	1.48 dys	Mod	39.08 dys	Mod	29.21 dys
	A2	-7.33 dys -33.6%	A2	-4.40 dys -47.1%	A2	-1.06 dys -72.0%	A2	-15.58 dys -39.9%	A2	-13.66 dys -46.7%
	B1	-4.53 dys -20.8%	B1	-2.69 dys -28.9%	B1	-.72 dys -48.8%	B1	-8.93 dys -22.9%	B1	-8.24 dys -28.2%
Average snowfall per event	Mod	4.94 cm	Mod	6.23 cm	Mod	4.17 cm	Mod	5.38 cm	Mod	6.11 cm
	A2	-0.16 cm -3.2%	A2	-0.52 cm -8.4%	A2	+.014 cm +3.4%	A2	-0.19 cm -3.6%	A2	-0.35 cm -5.7%
	B1	-0.15 cm -3.1%	B1	-0.26 cm -4.1%	B1	+.062 cm +14.9%	B1	-0.18 cm -3.4%	B1	-0.32 cm -5.3%
# days of snowpack per year	Mod	118.71 dys	Mod	27.80 dys	Mod	1.93 dys	Mod	136.88 dys	Mod	94.00 dys
	A2	-42.66 dys -35.9%	A2	-16.08 dys -57.9%	A2	-.141 dys -72.9%	A2	-47.59 dys -34.8%	A2	-47.29 dys -50.3%
	B1	-26.30 dys -22.2%	B1	-10.67 dys -38.4%	B1	-.98 dys -51.1%	B1	-26.97 dys -19.7%	B1	-28.49 dys -30.3%
Cumulative WSI	Mod	66.9	Mod	2.0	Mod	-11.4	Mod	94.9	Mod	52.5
	A2	28.2	A2	-6.4	A2	-16.3	A2	40.3	A2	11.5
	B1	40.4	B1	-3.5	B1	-14.0	B1	60.5	B1	25.5

Table 2. Same as table 1, except for five other LCC regions: Plains and Prairie Potholes, Great Plains, Gulf Coast Prairie, Upper Midwest and Great Lakes, and North Atlantic.

Originating group	Country	Model ID	Reference
Canadian Centre for Climate Modelling & Analysis	Canada	CGCM3.1	Flato <i>et al.</i> (2000)
Météo-France / Centre National de Recherches Météorologiques	France	CNRM-CM3	Déqué <i>et al.</i> (1994)
Commonwealth Scientific and Industrial Research Organisation (CSIRO) Atmospheric Research	Australia	CSIRO-Mk3.0	Gordon and O'Farrell (1997)
CSIRO Atmospheric Research	Australia	CSIRO-Mk3.5	Gordon <i>et al.</i> (2002)
United States Department of Commerce / National Oceanic and Atmospheric Administration (NOAA) / Geophysical Fluid Dynamics Laboratory	USA	GFDL-CM2.0	Delworth <i>et al.</i> (2006)
National Aeronautics and Space Administration (NASA) Goddard Institute for Space Studies	USA	GISS-ER	Schmidt <i>et al.</i> (2005)
Meteorological Institute of the University of Bonn, Meteorological Research Institute of Korea Meteorological Administration (KMA), and Model and Data group	Germany / Korea	MIUB ECHO-G	Legutke and Voss (1999)
Max Planck Institute for Meteorology	Germany	MPI ECHAM5	Roeckner <i>et al.</i> (2003)
Meteorological Research Institute	Japan	MRI-CGCM2.3.2	Kitoh <i>et al.</i> (1995)

Table 3. List of the nine global climate models analyzed in this study.

Figure 1

[Click here to download Rendered Figure: fig1.pdf](#)

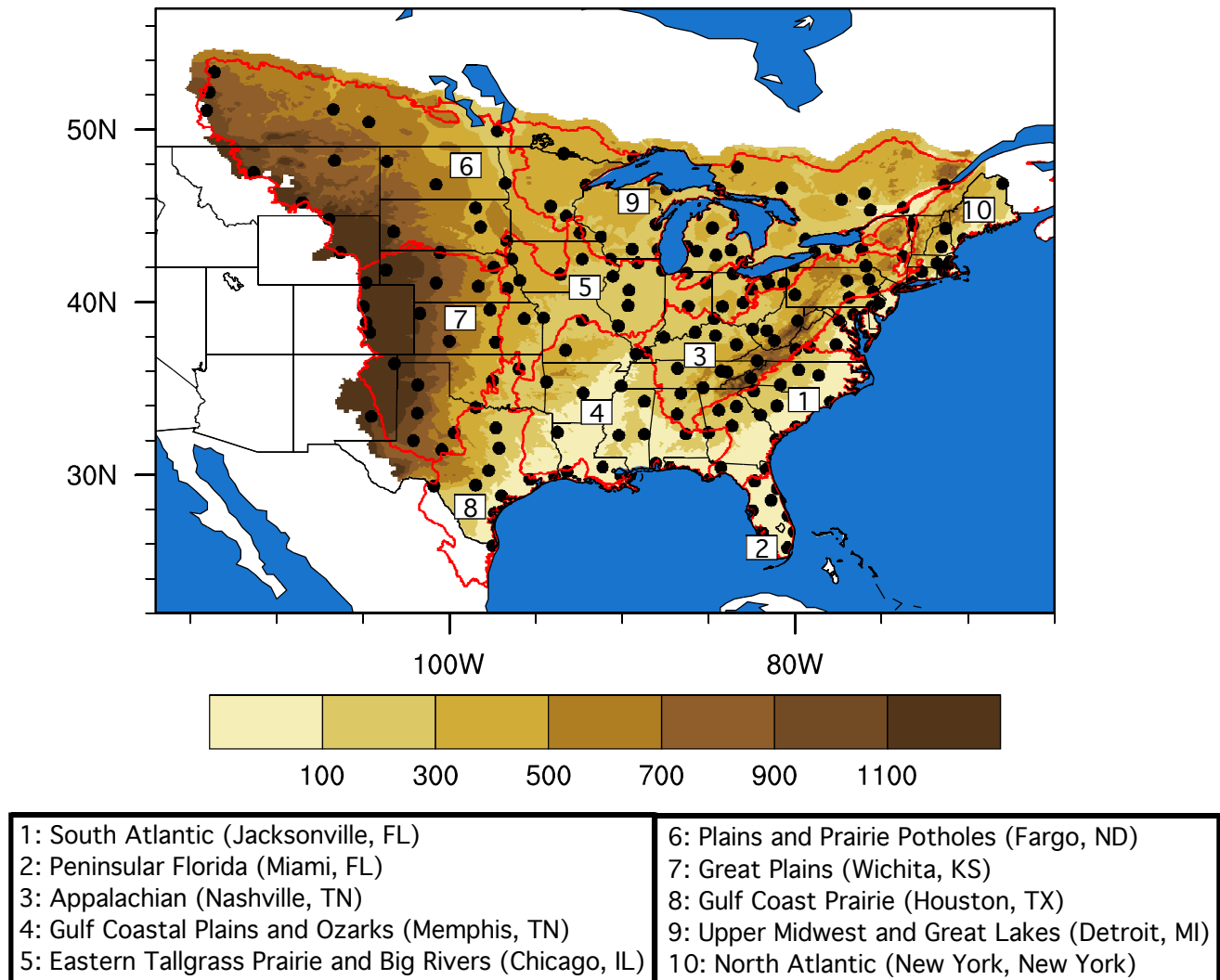


Fig. 1 Map of elevation (m), based on ETOPO2 global topographic grid, with red polygons outlining the relevant LCCs and black dots for 196 stations. Snowfall climatology at these stations is used to assess the performance of SNOW-17 and estimate the SCF parameter. The 10 LCC regions of interest are identified by number. For each LCC region, the largest populated city is identified.

Figure 2

[Click here to download Rendered Figure: fig2.pdf](#)

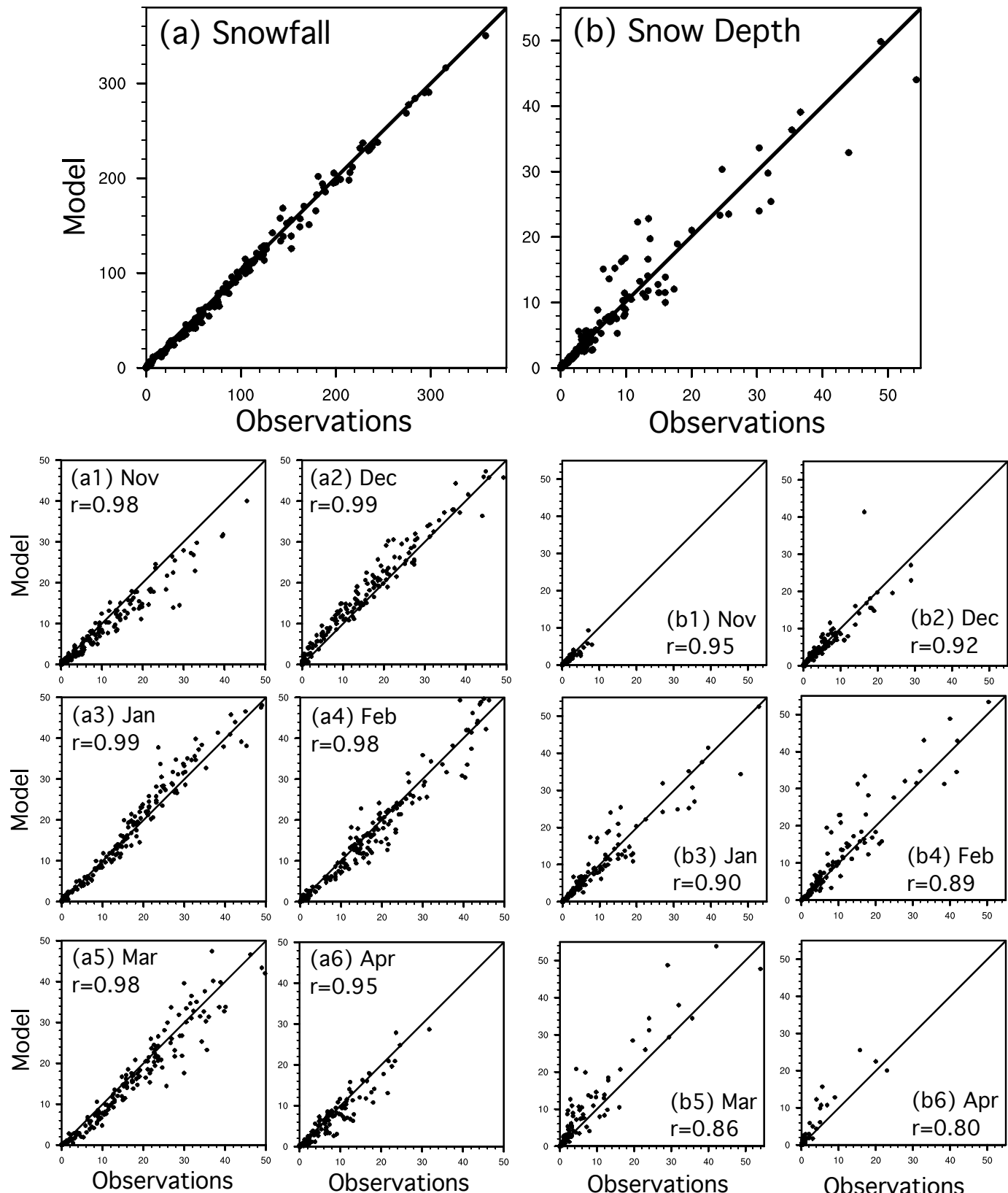


Fig. 2 Scatter plots of observed versus simulated (a) annual snowfall (cm) and (b) DJF snow depth for 196 stations, based on a climatology for 1981-2000. For snowfall (snow depth), the temporal correlation is 0.99 (0.90) and root-mean-square-difference is 5.9 cm (4.4 cm). Scatter plots for individual months are shown for (a1-6) snowfall and (b1-6) snow depth, with the correlation coefficient provided in each panel.

Figure 3

[Click here to download Rendered Figure: fig3.pdf](#)

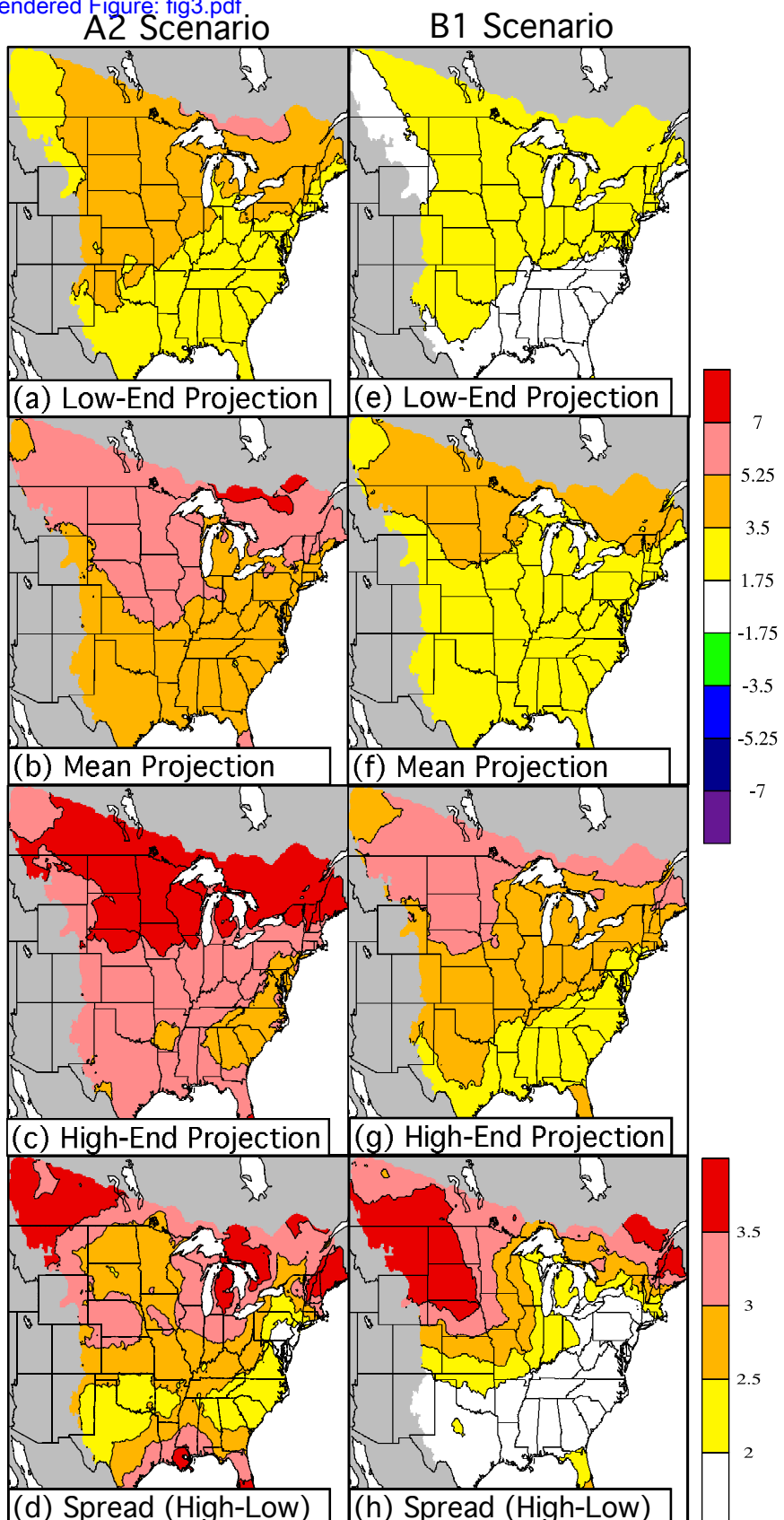


Fig. 3 Projected change in DJFM mean temperature ($^{\circ}\text{C}$) by the late 21st century, computed as the difference between 2081-2100 and 1981-2000. Results are shown for the (a-d) A2 and (e-h) B1 emission scenarios and are broken down by (a,e) low-end projection, (b,f) mean projection, (c,g) high-end projection, and (d,h) spread (difference between high-end and low-end projections) per grid cell. Among nine GCMs, the greatest warming at each grid cell is considered high-end and the least warming is considered low-end. The upper color bar pertains to (a-c, e-g) and the lower color bar pertains to (d,h). All of the differences shown in (a-c, e-g) are statistically significant ($p < 0.1$), except over central Montana and southern Alberta in (e).

Figure 4

[Click here to download Rendered Figure: fig4.pdf](#)

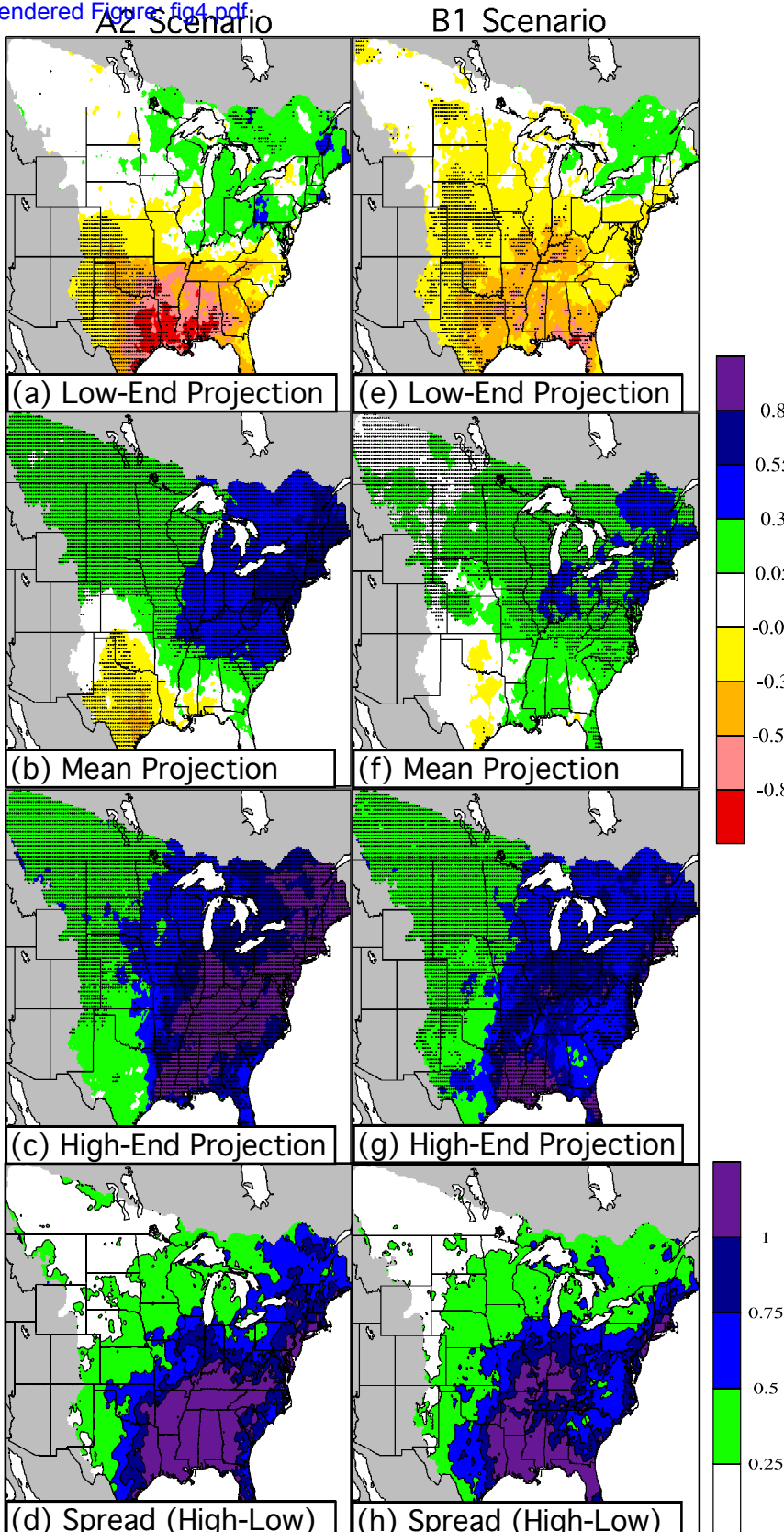


Fig. 4 Projected change in DJFM mean precipitation (mm/day) by the late 21st century, computed as the difference between 2081-2100 and 1981-2000. Results are shown for the (a-d) A2 and (e-h) B1 emission scenarios and are broken down by (a,e) low-end projection, (b,f) mean projection, (c,g) high-end projection, and (d,h) spread (difference between high-end and low-end projections) per grid cell. Among nine GCMs, the greatest increase in precipitation at each grid cell is considered high-end and the greatest drying (or least increase in precipitation) is considered low-end. The upper color bar pertains to (a-c, e-g) and the lower color bar pertains to (d,h). Statistically significant differences in (a-c, e-g) are dotted ($p<0.1$).

Figure 5

[Click here to download Rendered Figure: fig5.pdf](#)

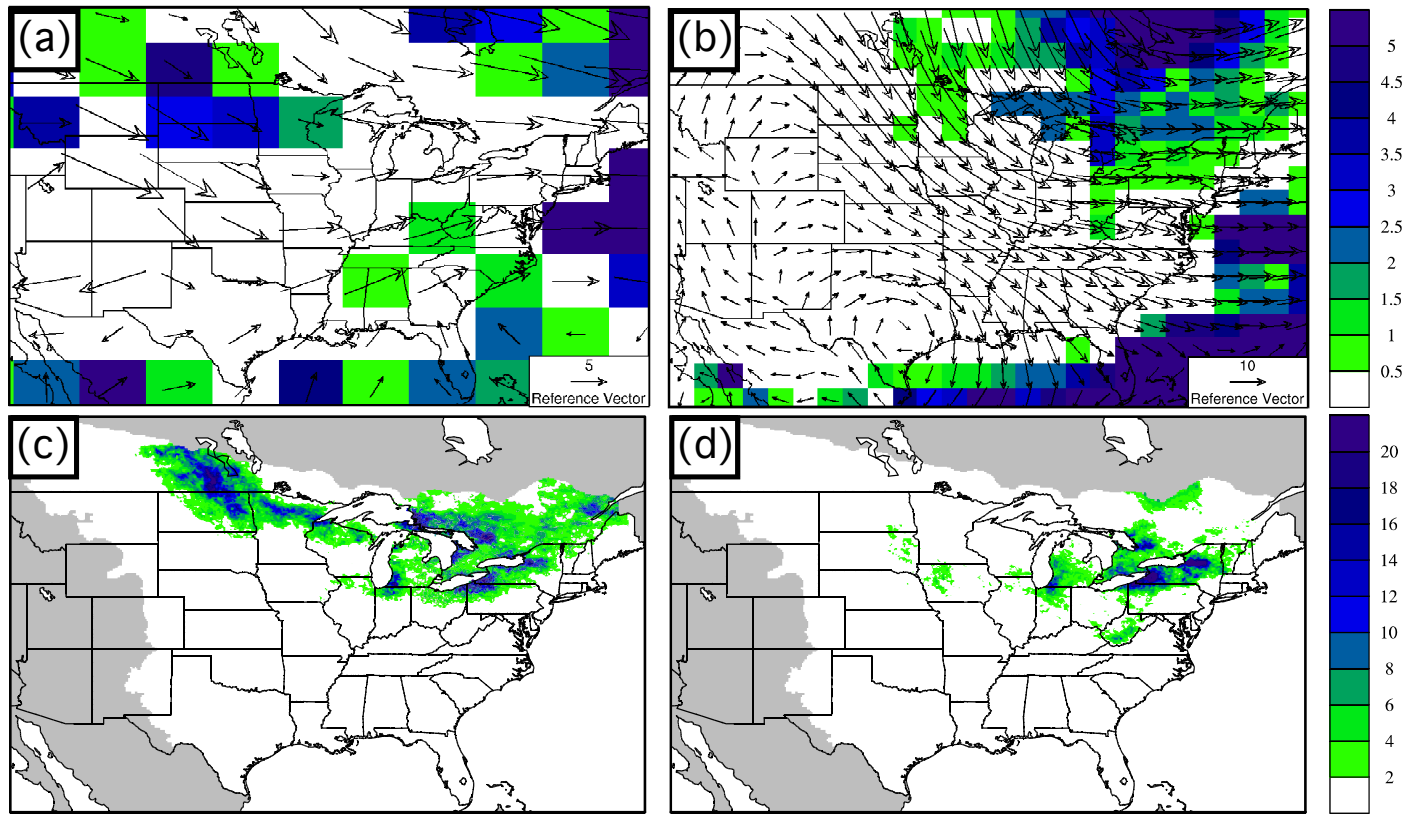


Fig. 5 Simulated daily precipitation (mm) and 850-hPa wind vectors from a select day in (a) December 1989 from the 20C3M simulation of GISS Model E-R and a select day in (b) December 1987 from the 20C3M simulation of MPI ECHAM5, which include northwesterly winds over the Great Lakes which should support lake-effect snowfall. Reference vectors are assigned values of (a) 5 m/s and (b) 10 m/s. For these two events, simulated snowfall (cm) is shown in (c) for the GISS model and (d) for the MPI model, based on SNOW-17 simulations forced by downscaled climate data. Lake-effect precipitation is absent in (a-b) but captured in (c-d).

Figure 6

[Click here to download Rendered Figure: fig6.pdf](#)

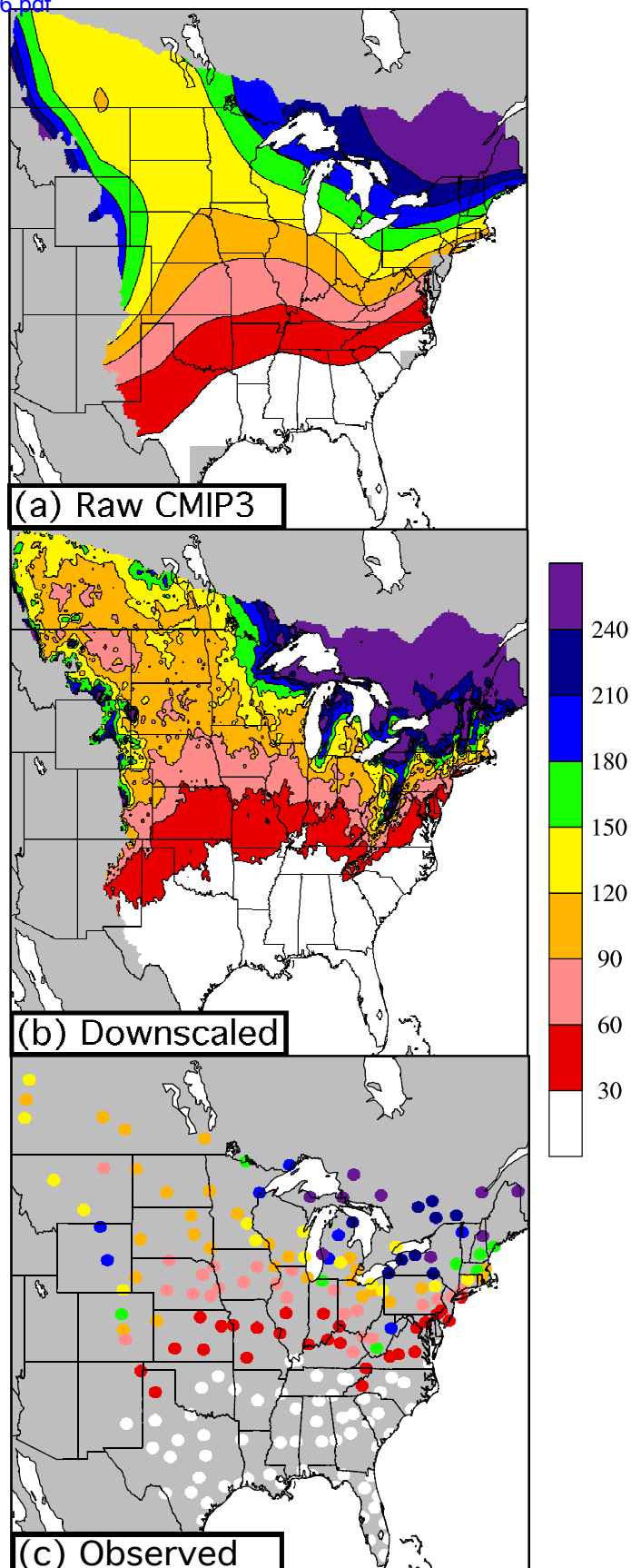


Fig. 6 Climatological mean annual snowfall (cm) from the (a) raw CMIP3 GCMs, (b) downscaled SNOW-17, and (c) 196 weather stations for 1981-2000. Since the GCMs only saved liquid-equivalent of snowfall, a 10:1 ratio was applied to crudely estimate simulated snowfall.

Figure 7

[Click here to download Rendered Figure: fig7.pdf](#)

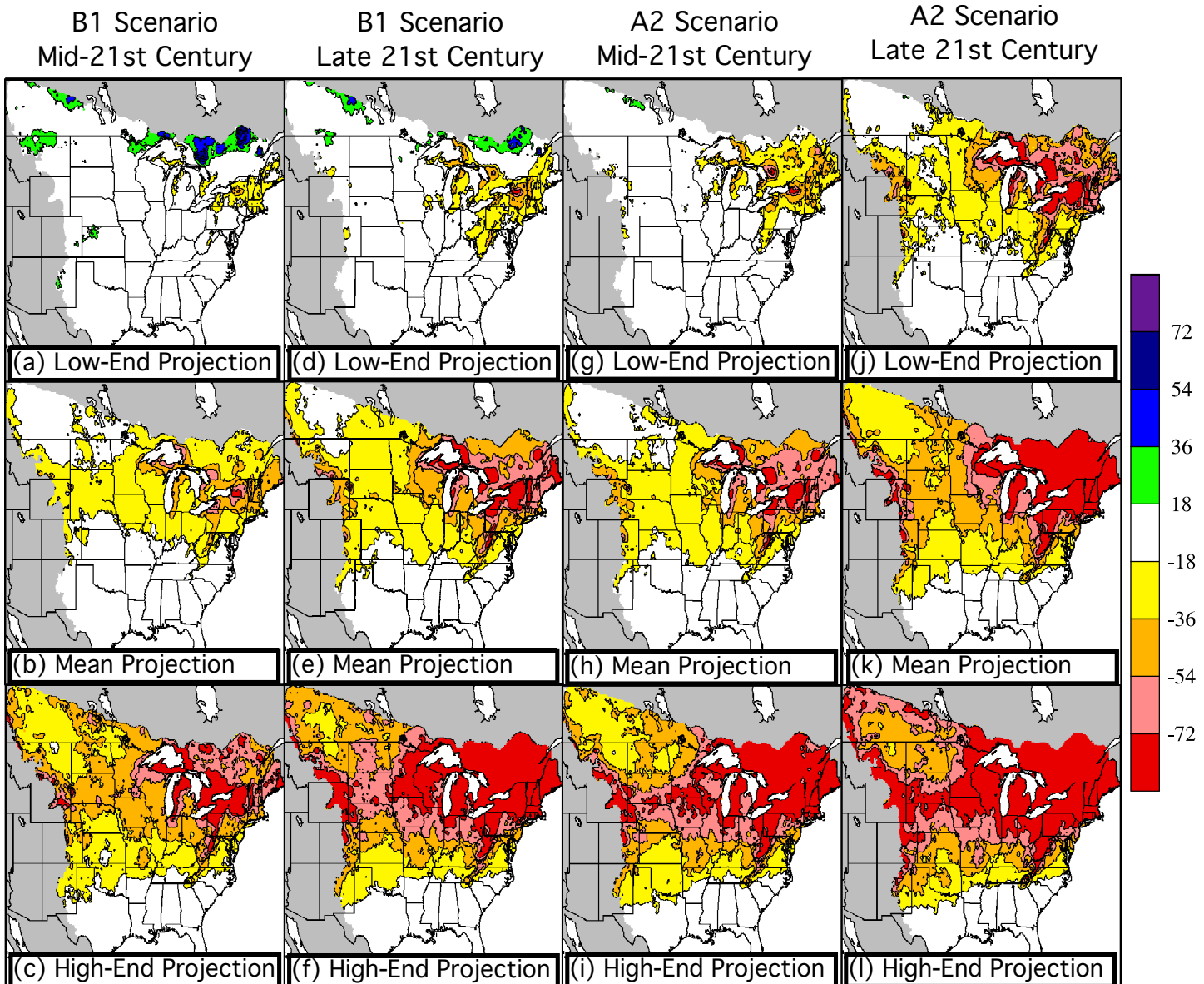


Fig. 7 Projected change in annual snowfall (cm) by the (a-c,g-i) mid-21st century (2046-2065) and (d-f,j-l) late 21st century (2081-2100), computed as the difference from the late 20th century (1981-2000), according to the (a-f) B1 and (g-l) A2 emission scenarios. Results are broken down by (a,d,g,j) low-end, (b,e,h,k) mean, and (c,f,i,l) high-end projections per grid cell. Among the nine GCMs, the largest decline in snowfall at each grid cell is considered high-end and the greatest increase (or smallest decline) is considered low-end.

Figure 8

[Click here to download Rendered Figure: fig8.pdf](#)

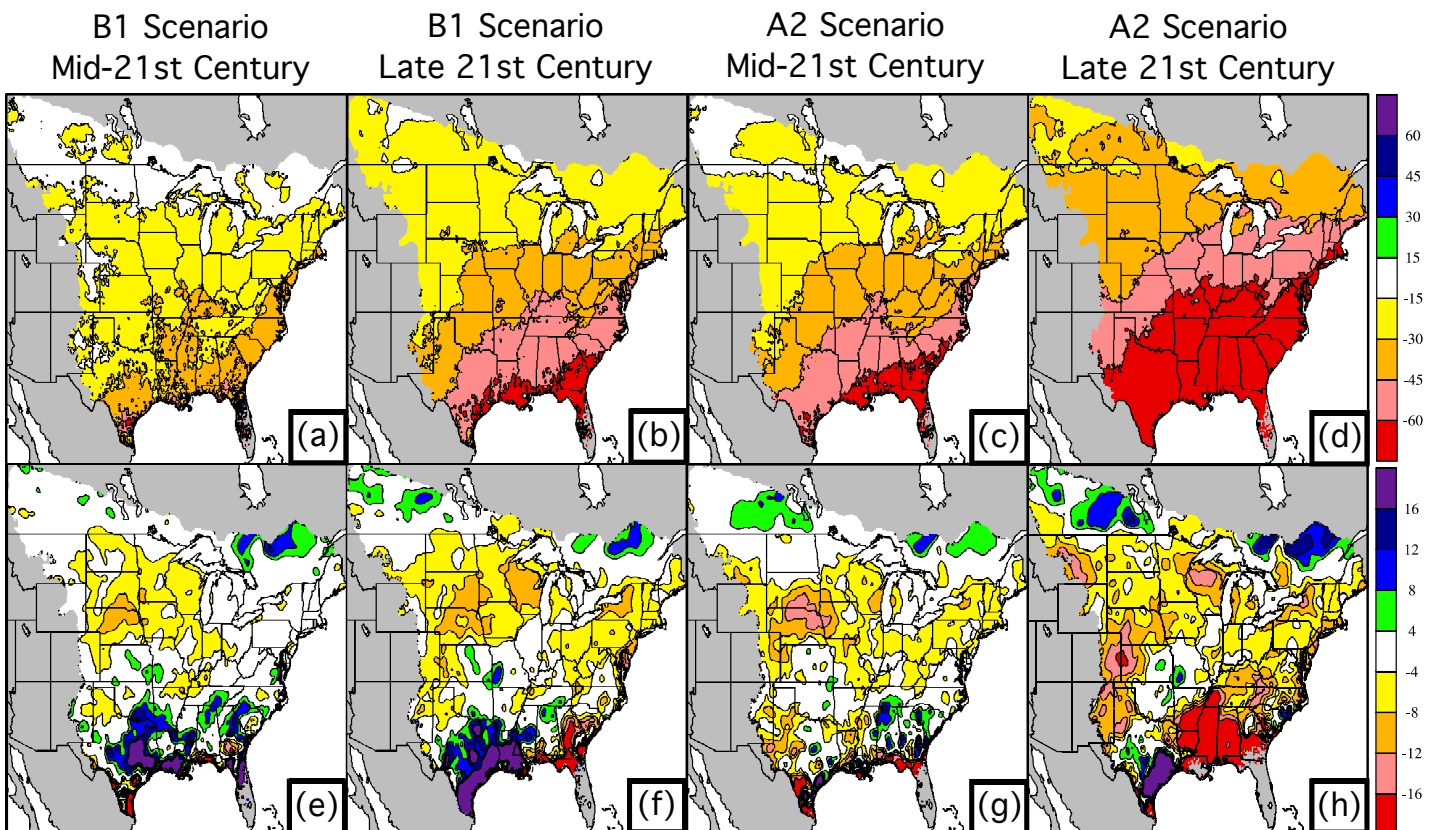


Fig. 8 Mean projected percentage change in the annual (a-d) frequency of daily snowfall events of at least 1 cm and (e-h) mean snowfall per event by the (a,e,c,g) mid-21st century (2046-2065) and (b,f,d,h) late 21st century (2081-2100), compare to the late 20th century (1981-2000). Results are shown both for the (a-b,e-f) B1 and (c-d,g-h) A2 emission scenarios. The median projections are also computed (not shown) and found to be quite consistent with the mean projections shown here.

Figure 9

[Click here to download Rendered Figure: fig9.pdf](#)

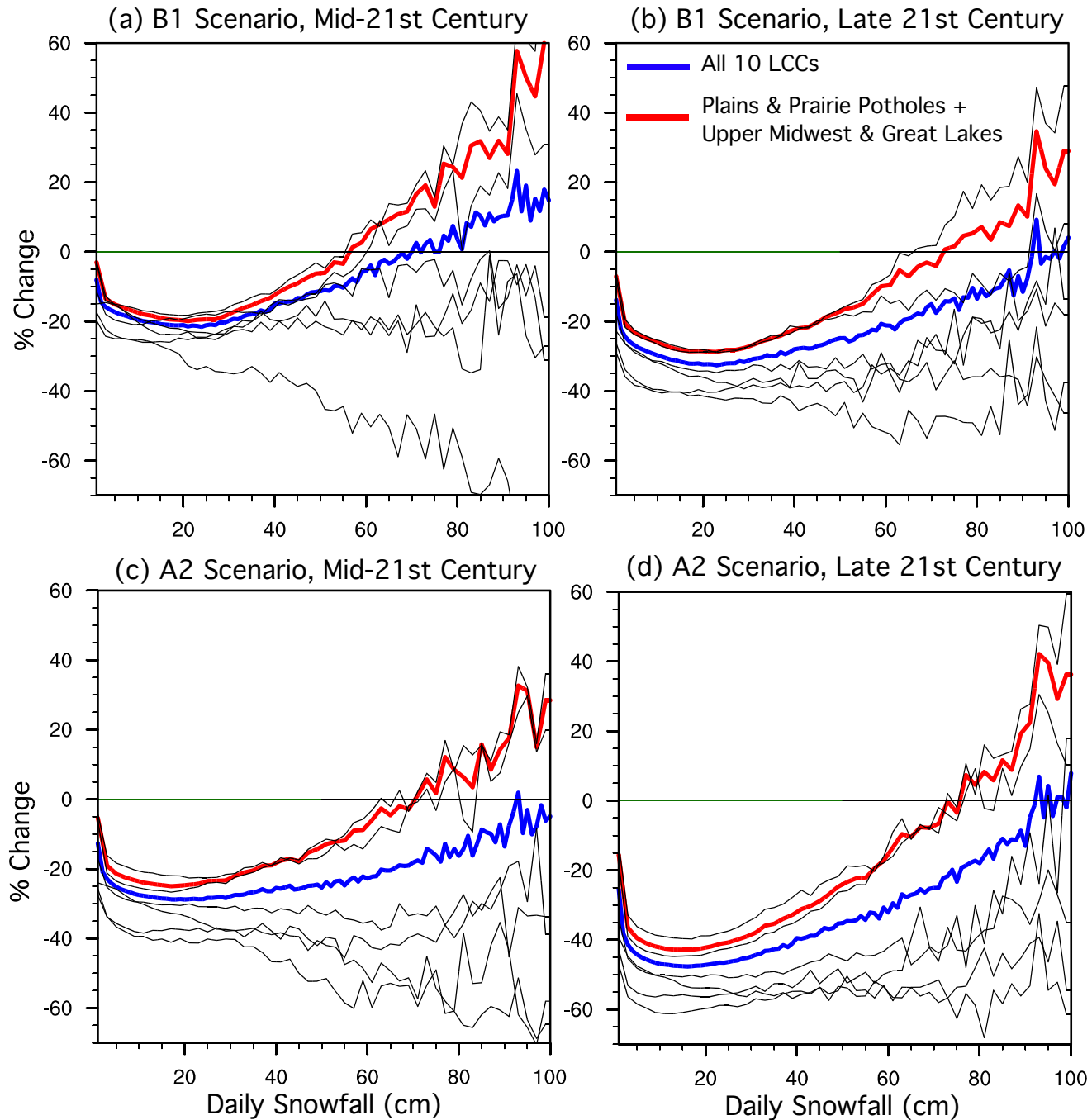


Fig. 9 Projected percentage change in the frequency of daily snowfall (cm) events, within the entire 10 LCC study region (blue lines) and the region encompassing the Plains and Prairie Potholes LCC and Upper Midwest and Great Lakes LCC (red lines). Projections are shown for the (a-b) B1 and (c-d) A2 scenarios and for the (a,c) mid-21st and (b,d) late 21st century. The x-axis consists of 1-cm daily snowfall bins (0.1-1, 1-2, 2-3,..., 99-100) for the former region and 2-cm bins (0.1-2, 2-4, 4-6,..., 98-100) for the latter region. Thin black curves are also included for each of the following LCC regions: Appalachian, Eastern Tallgrass Prairie and Big Rivers, Plains and Prairie Potholes, Great Plains, Upper Midwest and Great Lakes, and North Atlantic.

Figure 10

[Click here to download Rendered Figure: fig10.pdf](#)

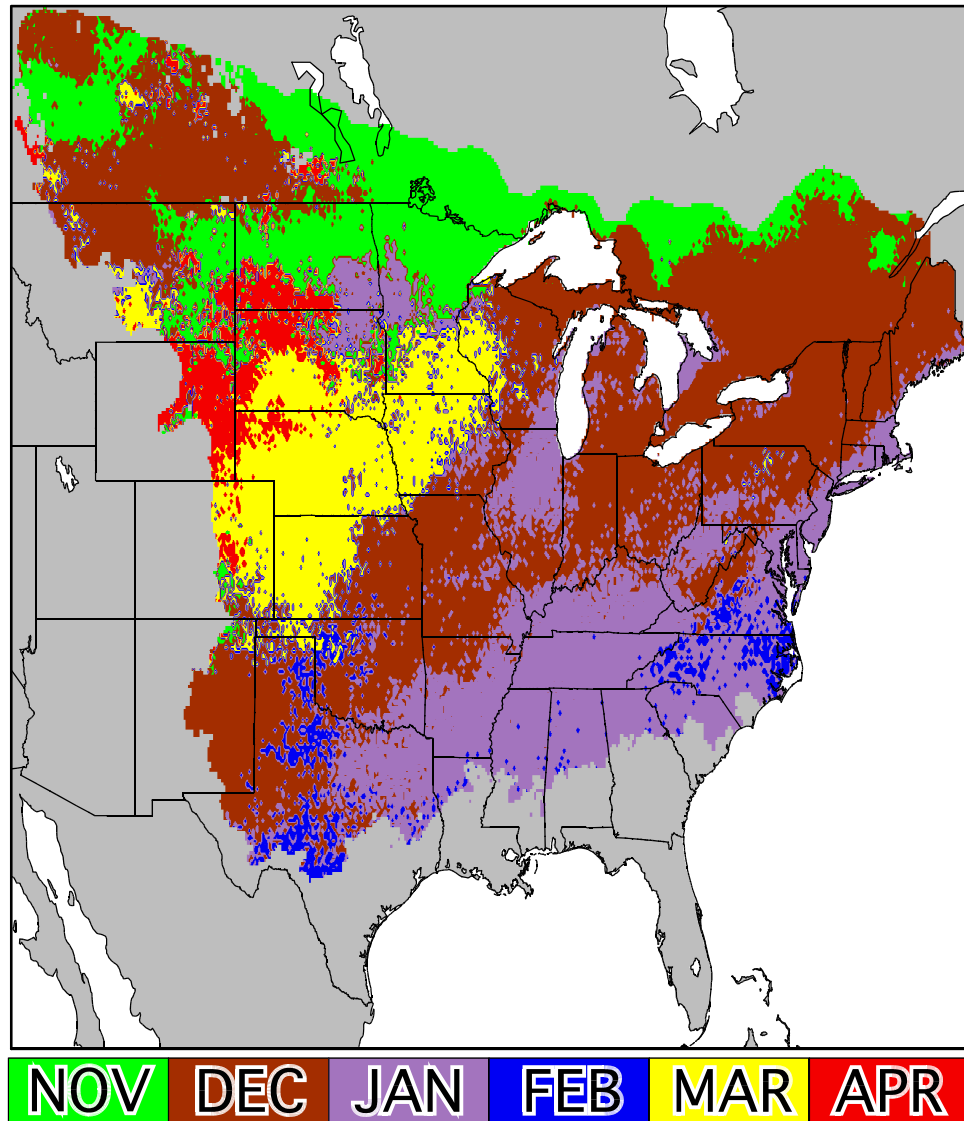


Fig. 10 Month of maximum projected decline in snowfall, according to the A2 emission scenario by the end of the 21st century (2081-2100), compared to the late 20th century (1981-2000). SNOW-17 is forced by downscaled climate projections from nine GCMs, the mean snowfall projection is computed among these models, and then the month of maximum decline in snowfall is identified.

Figure 11

[Click here to download Rendered Figure: fig11.pdf](#)

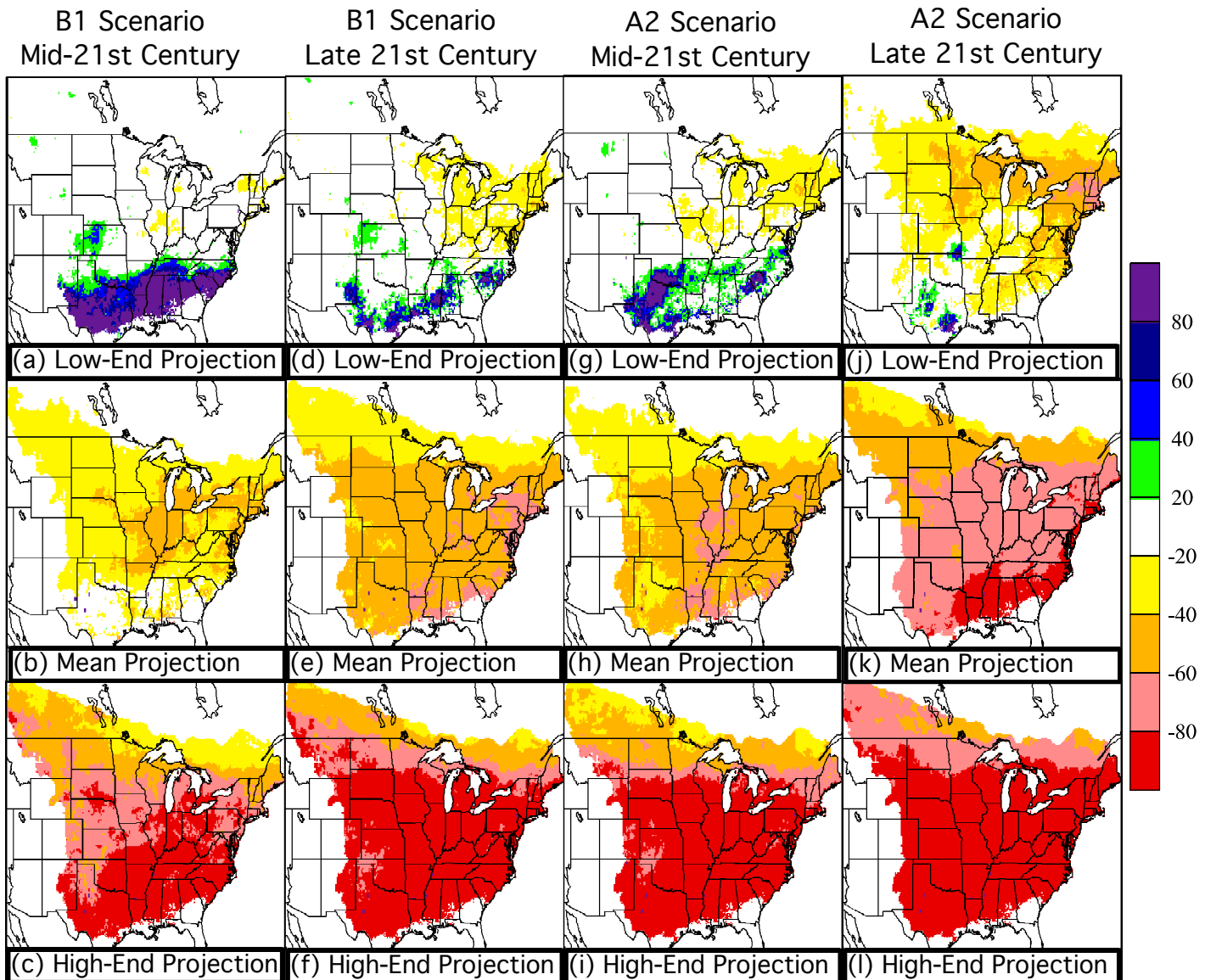


Fig. 11 Projected percentage change in NDJFMA mean snow depth by the (a-c,g-i) mid-21st century (2046-2065) and (d-f,j-l) late 21st century (2081-2100), computed as the difference from the late 20th century (1981-2000), according to the (a-f) B1 and (g-l) A2 emission scenarios. Results are broken down by (a,d,g,j) low-end, (b,e,h,k) mean, and (c,f,i,l) high-end projections per grid cell. Among the nine GCMs, the largest decline in snow depth at each grid cell is considered high-end and the greatest increase (or smallest decline) is considered low-end.

Figure 12

[Click here to download Rendered Figure: fig12.pdf](#)

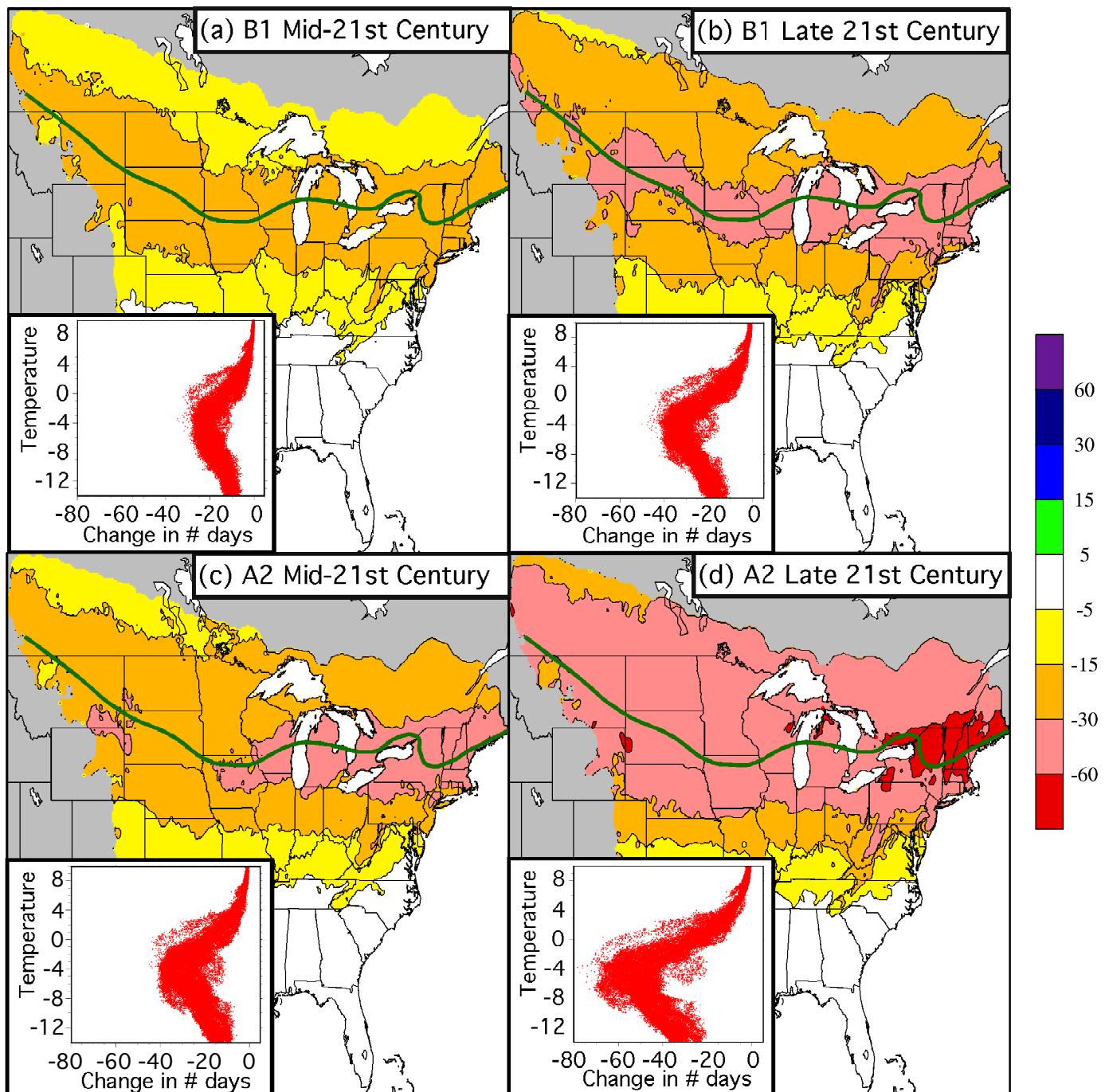


Fig. 12 Mean projected change in the number of days per year with a minimum snowpack of 1 cm by the (a,c) mid-21st century (2046-2065) and (b,d) late 21st century (2081-2100), compared to the late 20th century (1981-2000). Results are shown for the (a-b) B1 and (c-d) A2 emission scenarios. The green curve represents the -5°C mean isotherm for DJFM for 1981-2000. Scatter plots display (y-axis) mean climatological DJFM temperature ($^{\circ}\text{C}$) from 1981-2000 versus (x-axis) projected change in number of days per year with a minimum snowpack, with a dot for each grid cell

Figure 13

[Click here to download Rendered Figure: fig13.pdf](#)

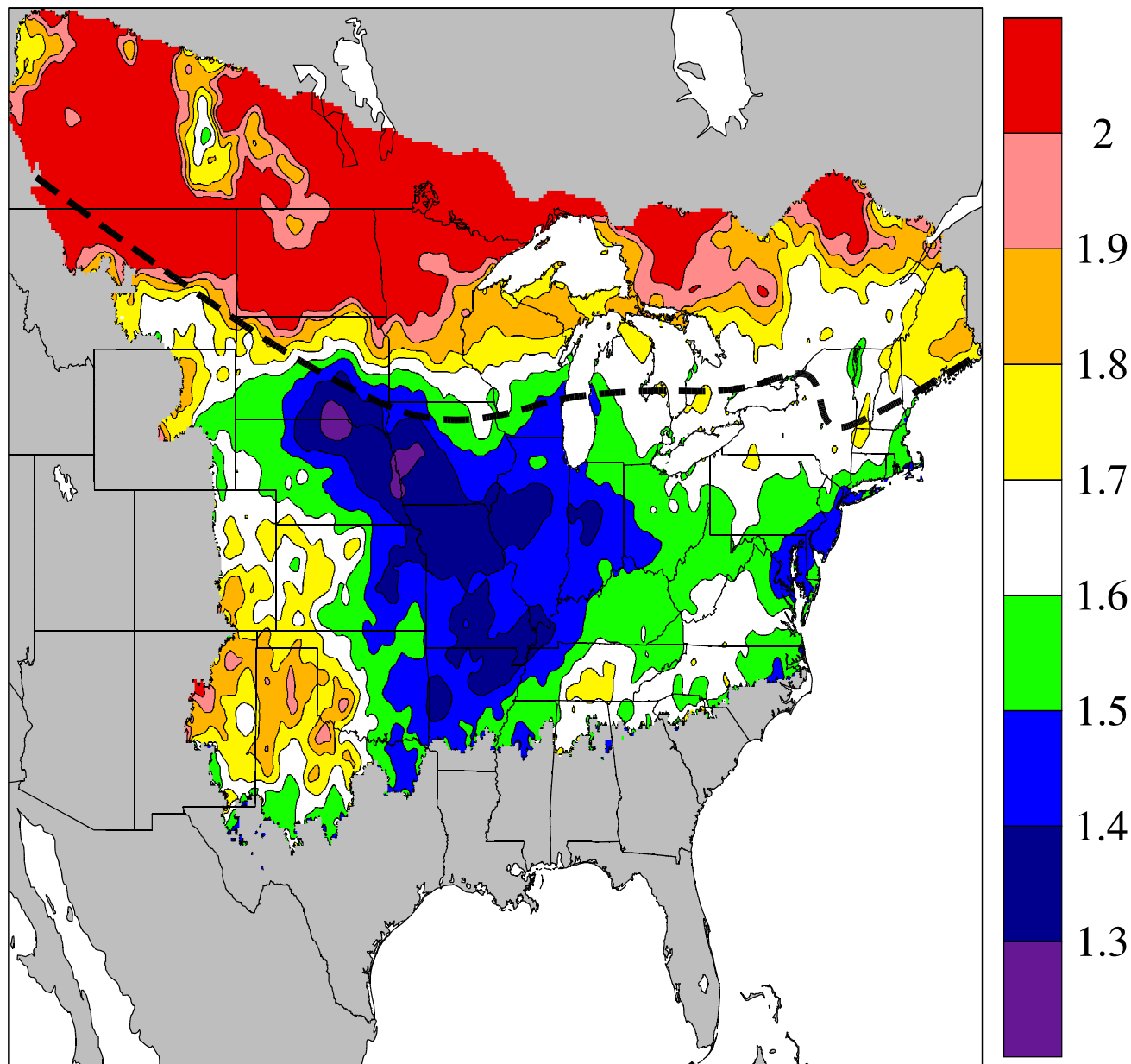


Fig. 13 Ratio of the mean projected change in annual snowfall by the late 21st century (2081-2100) to the mean projected change by the mid-21st century (2046-2065), compared to the 20th century (1981-2000). Results are based on the A2 emission scenario. Ratios greater than one indicate accelerated snowfall declines later in the 21st century. The black dashed line represents the -5°C mean isotherm for DJFM for 1981-2000.

Figure 14

[Click here to download Rendered Figure: fig14.pdf](#)

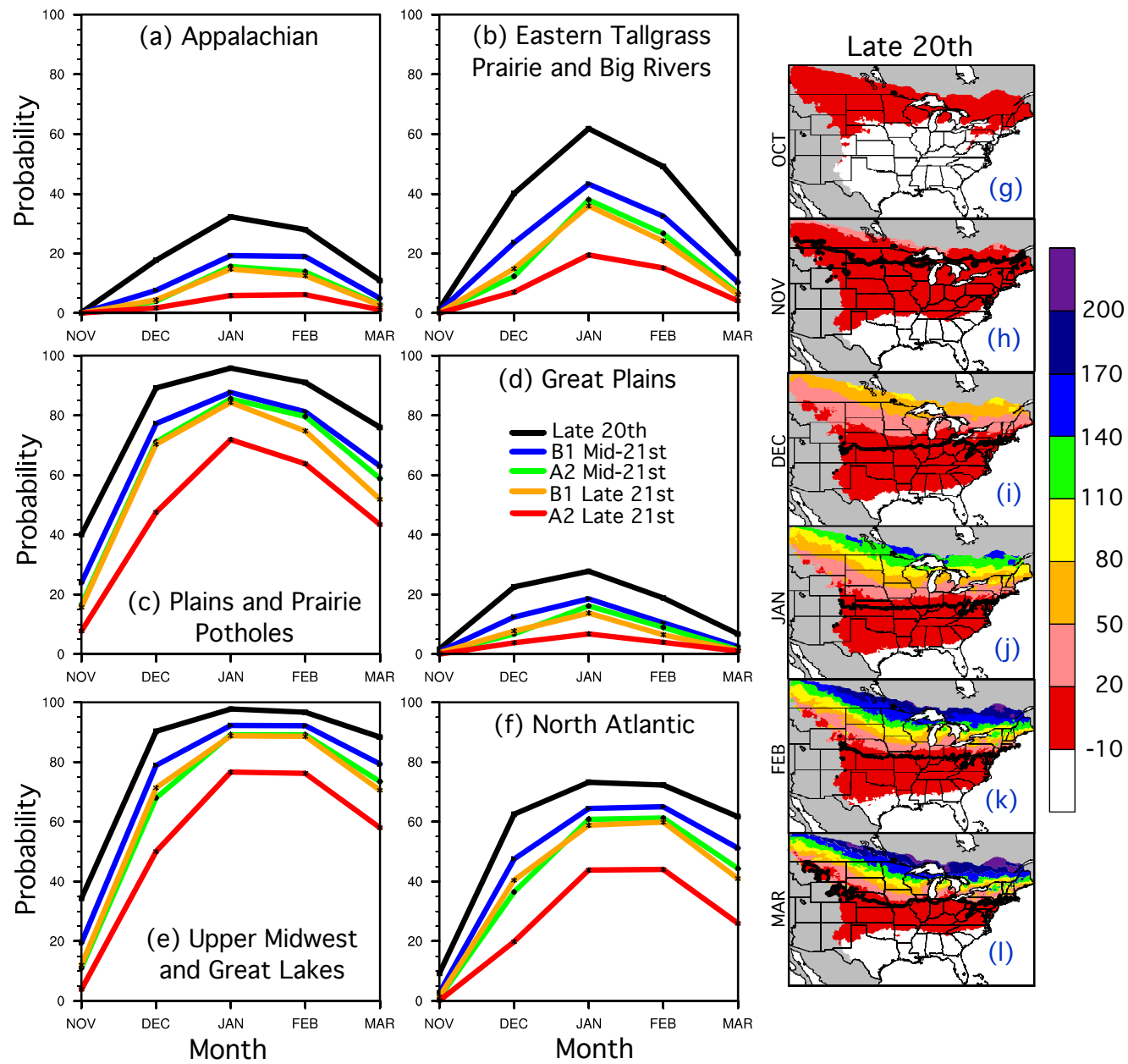


Fig. 14 (a-f) Mean probability of the daily CWSI in specific LCC regions exceeding 7.2 from November to March, for the late 20th century (black), mid-21st century (B1 scenario - blue, A2 scenario - green), and late 21st century (B1 - orange, A2 - red), based on mean projections from nine GCMs. (g-l) Mean CWSI for October-March for the late 20th century. The thick black lines indicate CWSI=7.2, a critical threshold for mallard ducks. Note that the CWSI is cumulatively summed each day from 1 September to 31 March.